UNIVERSITY OF TARTU

Faculty of Science and Technology
Institute of Technology

Faruq Olamilekan Ibrahim

Non-precious metal electrocatalysts for oxygen reduction via ionothermal synthesis

Bachelor's Thesis (12 ECTS)

Curriculum Science and Technology

Supervisor(s):
MSc Kaarel Kisand
Professor Kaido Tammeveski

Tartu 2024

Abstract

Non-precious metal electrocatalysts for oxygen reduction via ionothermal synthesis

The increasing global energy demand necessitates the development of sustainable energy technologies. Anion-exchange membrane fuel cells (AEMFCs) present a promising alternative to proton-exchange membrane fuel cells (PEMFCs) due to their ability to utilize platinum-group metal (PGM)-free catalysts, which significantly reduce costs and resource dependency. This thesis focuses on the synthesis, characterization, and performance evaluation of transition metal and nitrogen-doped carbon catalysts for AEMFCs. Utilizing cyclodextrine and magnesium nitrate, various PGM-free catalysts were developed, and the synthesis conditions were optimized. The catalysts were investigated with both physical and electrochemical characterization techniques. The catalysts' performance was assessed through rotating disk electrode (RDE) measurements and single-cell AEMFC tests. The optimized FeNC-CD3 catalyst exhibited a peak power density of 596 mW cm^{-2}, showcasing its potential as a viable alternative to conventional Pt-based catalysts. This work highlights the critical role of hierarchical porosity in enhancing oxygen reduction reaction (ORR) activity and paves the way for the development of cost-effective and efficient AEMFC technologies.

Keywords: Anion-exchange membrane fuel cells (AEMFCs), PGM-free catalysts, oxygen reduction reaction (ORR), M-N-C catalysts

CERCS: Electrochemistry

Ionotermiliselt sünteesitud väärismetallivabad katalüsaatorid hapniku redutseerumisreaktsiooni jaoks

Lühikokkuvõte:

Kasvav ülemaailmne energianõudlus nõuab uute energiatehnoloogiate väljatöötamist. Anioonvahetusmembraaniga kütuseelement on paljulubav alternatiiv prootonvahetusmembraaniga kütuseelemendile, kuna seal on võimalik kasutada väärismetallivabasid katalüsaatoreid. Antud lõputöö keskendub siirdemetalli ja lämmastikuga dopeeritud süsinikkatalüsaatorite sünteesile, füüsikalis-keemilisele iseloomustamisele ja elektrokatalüütilise aktiivsuse hindamisele. Materjalid sünteesiti ionotermilise meetodi abil, kasutades tsüklodekstriini ja magneesiumnitraati. Sünteesitingimusi optimeeriti ja valmistatud katalüsaatoreid uuriti erinevate meetoditega (SEM, STEM, BET, XPS ja XRD) ning nende elektrokatalüütilist aktiivust hapniku elektroredutseerumisel uuriti põhjalikult kasutades pöörleva ketaselektroodi (RDE) mõõtmisi. Parima katalüsaatoriga viidi läbi mõõtmine kütuseelemendis, kus saavutati maksimaalne võimsustihedus 596 mW cm^{-2}.

TABLE OF CONTENTS

ABBREVIATIONS

AEM	Anion-Exchange Membrane
AEMFC	Anion-Exchange Membrane Fuel Cell
BET	Brunauer-Emmett-Teller
BF	Bright Field
CDC	Carbide-Derived Carbon
CNT	Carbon Nanotubes
EDX	Energy-Dispersive X-ray Spectroscopy
E_{onset}	Onset Potential
$E_{1/2}$	Half-Wave Potential
FCEV	Fuel Cell Electric Vehicle
HAADF	High-Angle Annular Dark-Field
K-L	Koutecky-Levich
LSV	Linear Sweep Voltammetry
MEA	Membrane Electrode Assembly
M-N-C	Metal-Nitrogen-Carbon
NC	Nitrogen-Doped Carbon
M@NC	Nitrogen-Doped Carbon with Metal
NPMCs	Non-Precious Metal Catalysts
ORR	Oxygen Reduction Reaction
PEFC	Polymer electrolyte fuel cells
PEMFC	Proton-Exchange Membrane Fuel Cell
PGM	Platinum Group Metal
PSD	Pore Size Distribution
RDE	Rotating Disk Electrode
RHE	Reversible Hydrogen Electrode
SEM-EDX	Scanning Electron Microscopy with Energy-Dispersive X-ray Analysis
SD	Site Density
S_{DFT}	Specific surface area
STEM	Scanning Transmission Electron Microscopy
XAS	X-ray Absorption Spectroscopy
XPS	X-ray Photoelectron Spectroscopy
XRD	X-ray Diffraction

INTRODUCTION

Addressing the carbon energy cycle, which is causing environmental harm and negatively impacting global living conditions, stands out as a key priority for humanity in the 21st century. As per the International Energy Agency, global energy consumption is on the rise at an annual rate of 1%, and the transportation sector is swiftly emerging as the most substantial energy industry (Ratso, 2020). Nevertheless, as stated by Nazir et al., (2020) a predominant portion of the global transportation industry, encompassing airplanes, trains, and automobiles, relies solely on fossil fuels, including gasoline, diesel, and kerosene. Fuel cells with polymer electrolyte membranes have become a viable approach for mitigating CO_2 emissions in automotive applications and have already been extensively employed in fuel cell electric vehicles (FCEV) (Wagner et al., 2010).

Fuel cells have the ability to generate electricity by converting chemical energy from fuel and oxidant, with the help of continuous supply of hydrogen. According to Shao et al., (2016) when hydrogen is utilized as the fuel, the fuel cell generates electricity, water, and a moderate amount of heat. There are two main types of low temperature fuel cells, however the polymer electrolyte fuel cells (PEFC), which is either the proton exchange membrane fuel cell (PEMFC) or anion exchange membrane fuel cell (AEMFC) is most promising for mobile applications. In the PEMFC, both the cathode and anode contain platinum-based catalysts. At the anode, the hydrogen is oxidized and at the cathode oxygen is reduced. On these electrodes (cathode), there are highly dispersed Pt nanoparticles, which serve as catalysts that drive the reaction rate of the reduction and oxidation reactions. Unfortunately, platinum is scarce and costly noble metal, as such much research has gone into finding alternative catalysts.

AEMFCs are increasingly being recognized as a promising alternative to PEMFCs. This is primarily due to their ability to utilize platinum-group metal (PGM)-free electrocatalysts at the cathode. Recent advancements have significantly enhanced the performance of AEMFCs, allowing them to reach performance levels comparable to PEMFCs that rely on platinum-based catalysts. These performance improvements are largely attributed to the development of anion-exchange membranes (AEMs) that offer superior ionic conductivity and stability.

This leads to the aim of this thesis which is to explore the development and optimization of platinum group metal-free (PGM-free) catalysts for AEMFCs, focusing on the synthesis and characterization of and the evaluation of their performance in fuel cells.

1 LITERATURE OVERVIEW

1.1 Polymer electrolyte fuel cells

A fuel cell is a device that converts fuel, like hydrogen, and oxidant, such as air, into electricity, heat, and typically water as a byproduct (Figure 1). There are five primary types of fuel cells currently in commercial use: 1) polymer electrolyte fuel cells (PEFC), 2) alkaline fuel cells, 3) solid oxide fuel cells, 4) molten carbonate fuel cells, and 5) phosphoric acid fuel cells. PEFCs are further divided into proton exchange membrane fuel cells (PEMFC), anion exchange membrane fuel cells (AEMFC), direct methanol fuel cells (DMFC) and direct ethanol fuel cells (DEFC). For instance, a proton exchange membrane fuel cell (PEMFC), a subtype of PEFC, operates via the overall reaction:

$$2H_2 + O_2 \rightarrow 2H_2O \quad (1)$$

Hydrogen is oxidized at the anode while oxygen is reduced at the cathode, producing water. The protons from the oxidized hydrogen travel through a proton exchange membrane (PEM) to the cathode, where they combine with oxygen to form water. Since the membrane is an electrical insulator, electrons flow through an external circuit, allowing them to do useful work.

A fuel cell consists of the membrane-electrode assembly (MEA), which are catalysts layers deposited onto carbon gas diffusion layers (GDLs), forming the anode and cathode (see Figure 1). These electrodes are then combined with a polymeric membrane. The MEA is then placed between bipolar flow field plates, which create additional pathways for the transport of gases and water vapor, while also providing structural integrity to the fuel cell stack. These flow field plates are usually made from graphite.

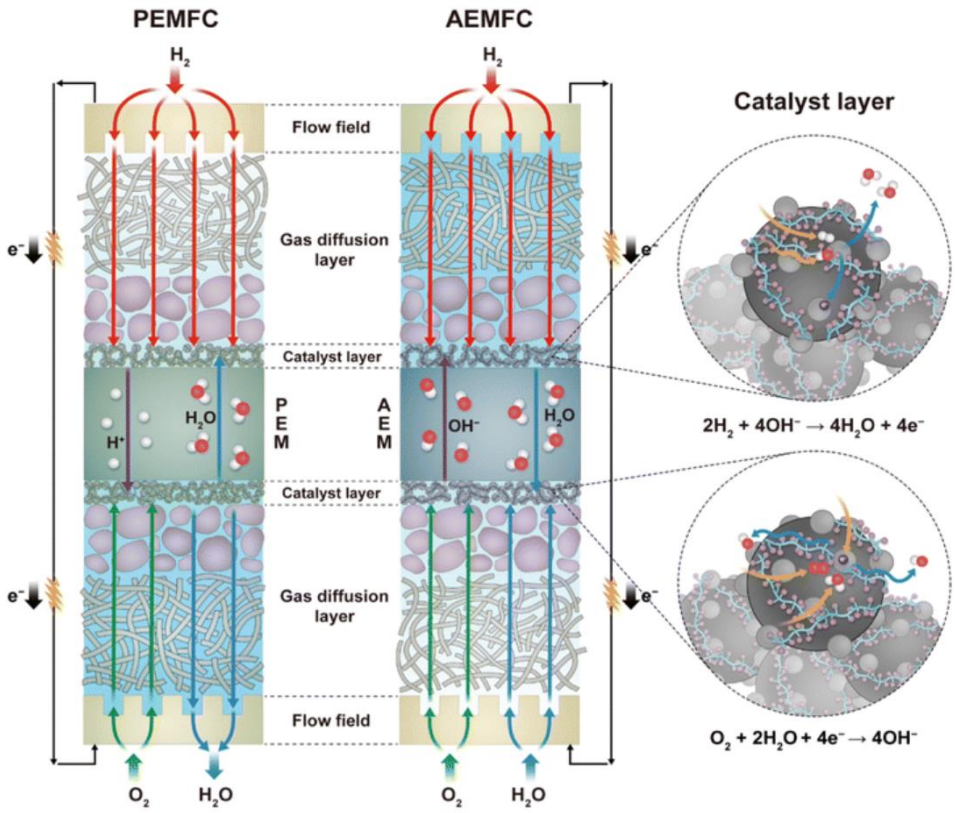

Figure 1. Schematics of a proton-exchange membrane fuel cell (PEMFC) and an AEMFC, adapted from (Hyun & Kim, 2023)

1.2 AEMFCs using non-precious metal cathode catalysts

Anion exchange membrane fuel cells (AEMFC) technology is relatively less developed compared to the well-established PEMFC technology, primarily due to the challenges in achieving comparable ionic conductivities for OH^- as for H^+ and the low chemical (and mechanical) stabilities of anion exchange membranes and ionomers at high pH, along with their susceptibility to carbonation. However, significant progress has been made in the past decade in addressing these issues, resulting in AEMFCs with performances on par with or even surpassing those of PEMFCs, albeit with CO_2 -free air (Mustain, 2018). The field of AEMFCs has witnessed substantial growth in recent years (Dekel, 2018; Gottesfeld et al., 2018). As discussed earlier, the oxygen reduction reaction (ORR) in alkaline conditions is more facile, allowing various non-precious metal catalysts (NPMCs) to efficiently catalyze the ORR (He & Cairns, 2015; Osmieri et al., 2018). Sarapuu et al. recently reviewed the application of metal-nitrogen-carbon (M-N-C) type catalysts and heteroatom-doped nanocarbon catalysts as cathode materials in AEMFCs (Sarapuu et al., 2018). Additionally, oxides such as MnO_2 and Co_3O_4, as well as spinels, cobalt ferrite, and silver, have demonstrated significant performances in AEMFCs or alkaline conditions, alongside carbon-based catalysts (J. Guo et al., 2010).

Comparison of the performances of different NPMCs achieved with various AEMs and AEIs, such as the Nafion™ standard in PEMFCs, is challenging due to the lack of standardized materials. Typically, the activity is compared to a benchmark platinum supported on carbon (Pt/C) catalyst, although certain types of ionomers are known to enhance the ORR activity of Pt/C (Ong et al., 2015). Therefore, rotating disk electrode (RDE) results are commonly reported as well. The ORR activity of carbon-based catalysts has steadily increased over the past decade, with M-N-C catalysts showing remarkable improvements from a kinetic current density j_k at 0.8 V vs reversible hydrogen electrode (RHE) of 1.5 mA cm^{-2} to up to 32 mA cm^{-2} at 0.8 V in rotating disk electrode (RDE) studies (He et al., 2012). In real MEAs, the increase in maximum power density has also been significant, rising from <100 mW cm^{-2} to over 1 W cm^{-2}. However, it is challenging to determine the exact contributions from system-level enhancements versus advances in catalysts (Dekel, 2018; Santori et al., 2020). In MEAs, a common issue with M-N-C materials is the active site density, necessitating higher amounts of catalytic centers and hierarchical porosity to enhance fuel cell performance (Santori et al., 2020). While some studies have opted to rely solely on nitrogen moieties, fuel cell studies on such materials are limited and often exhibit lower activities than those incorporating metals (Dai et al., 2015).

1.3 Oxygen reduction reaction

The electroreduction of oxygen is an important electrochemical process, playing a key role not only in energy production via fuel cells but also in biological respiration.

In alkaline conditions the ORR can proceed via two pathways. The 4-electron pathway:

$$O_2 + 2H_2O + 4e^- \rightarrow 4OH^- \quad (2)$$

or 2-electron pathway:

$$O_2 + H_2O + 2e^- \rightarrow HO_2^- + OH^- \quad (3)$$

followed by further reduction of HO_2^-

$$HO_2^- + H_2O + 2e^- \rightarrow 3OH^- \quad (4)$$

or disproportionation

$$2HO_2^- \rightarrow 2OH^- + O_2 \quad (5)$$

In fuel cell applications, the $4e^-$ pathway is generally preferred to avoid the possible degradation of fuel cell components caused by hydrogen peroxide or hydroperoxide anions, which are intermediates in the $2e^-$ pathway before breaking down into H_2O.

1.4 Oxygen reduction on non-precious metal catalysts

In the early 1960s, Willard Thomas Grubb and Leonard Niedrach of General Electric (GE) developed proton exchange membrane fuel cells for the Gemini missions. Although successful, the extensive platinum required for GE's fuel cells hindered their commercial viability. Recently, PEFC adoption has surged, with major automotive companies like Toyota, Hyundai, Honda, Ford, Chevrolet, and Mercedes-Benz introducing their own PEM fuel cell vehicles. Additionally, Plug Power, a hydrogen-powered forklift manufacturer, saw significant revenue in 2019. Despite these advancements, all these technologies still depend on Pt-based catalysts. The main issue with platinum is its limited global supply, with only 192.5 tons produced in 2019 out of an estimated 69,000-ton supply (Matthey, 2019). For example, a Toyota Mirai, the most produced FCEV, requires 35 grams of Pt for its fuel cell. At the current rate, replacing the entire global car fleet with FCEVs like the Mirai would take over 18 years, necessitating a nearly 100% recycling rate for Pt in the long term. Additionally, the high cost of FCEVs compared to conventional internal combustion engine vehicles presents a competitiveness challenge. Pt mining, primarily occurring in deep South African mines (Bushveld complex), further complicates cost concerns and supply stability issues. Despite progress in enhancing Pt-based catalysts' efficiency, integrating these improvements into full-size fuel cell stacks remains difficult. Even with optimistic projections, an ultimate Pt loading of 0.1 g kW^{-1} would still demand a significant portion of Earth's Pt reserves for PEFC technology. Consequently, the US Department of Energy has begun focusing on non-precious metal catalysts (NPMCs) in recent PEMFC roadmaps (Thompson & Papageorgopoulos, 2019). The quest for Pt alternatives began before PEFCs, with early research investigating bio-inspired cobalt phthalocyanine (CoPc) catalysts (Jasinski, 1965). Over time, the approach of utilizing carbon supports to enhance catalyst utilization has become crucial for both precious and non-precious metal catalysts (Banham & Ye, 2017; Osmieri et al., 2021; Shao et al., 2016). Further innovations, such as high-temperature treatments and using simple nitrogen sources and metal salts, have led to the development of some of the best NPMCs to date (Gupta et al., 1989; Jahnke et al., 1976). However, the precise nature of the active sites for the ORR after pyrolysis remains a subject of ongoing research (Matanovic et al., 2018; Mineva et al., 2019; Strickland et al., 2015).

1.4.1 Preparation of metal-nitrogen-carbon (M-N-C) catalysts

Metal-nitrogen-carbon catalysts are composed of a transition metal, nitrogen, and carbon. The carbon component provides chemical stability, electrical conductivity, a porous structure, and

mechanical strength. Traditionally, high surface area carbon materials like Vulcan carbon XC72 and Black Pearls BP2000 have been extensively used as support materials for heterogeneous catalysts, particularly as carriers for Pt nanoparticles (Shao et al., 2016; Yeager, 1984). However, carbon on its own has limited activity for the ORR. To create active sites for the ORR without using platinum, doping carbon with transition metals and nitrogen has proven to be the most effective approach (Shao et al., 2016). For unpyrolyzed transition metal phthalocyanines, the activity of metals decreases in the following order: Fe > Co > Ni > Cu > Mn (Zagal & Bedioui, 2016). However, since most catalysts undergo pyrolysis, the nature of the active site differs significantly from that of pure metal phthalocyanines (Tammeveski & Zagal, 2018; Zagal & Koper, 2016), resulting in different activity patterns. Before exploring the specifics of the active site, it is essential to understand the synthesis process of these materials.

The most prevalent methods for fabricating M-N-C catalysts include:

1) **The carbon doping method:** This involves pyrolyzing a synthesis mixture comprising a carbon carrier, nitrogen dopant (either a polymer or a small molecule with a high density of N atoms), and a transition metal source (typically an inexpensive salt) to introduce dopants into the carbon material. The nitrogen and metal sources may be combined, such as a macrocyclic compound containing the desired metal. These precursors are typically mixed either in liquid (e.g., sonication, stirring in a solvent) or solid phase (e.g., grinding, mixing, ball-milling), followed by pyrolysis at elevated temperatures to fuse them together, altering the chemical nature of the dopants and the substrate to create ORR-active sites (Bashyam & Zelenay, 2006; Ferrandon et al., 2012).

2) **The in situ doping method:** Similar to the method above, but the doped carbon network forms during pyrolysis from carbon, nitrogen, and transition metal sources. This method can yield a higher concentration of nitrogen and metals compared to method 1 above but presents challenges in controlling the structure and porosity of the final catalyst. This limitation is often mitigated by using well-defined structural precursors, such as metal-organic frameworks (Jia et al., 2015; Proietti et al., 2011; Strickland et al., 2015; Zitolo et al., 2015a), metal macrocycles (Kramm et al., 2016; Zagal & Bedioui, 2006), macrocyclic aerogels (Zion et al., 2020), or polymers (Jiang et al., 2018; X. Wang et al., 2016).

Research on M-N-C electrocatalysts for ORR has primarily focused on two main types of active sites: single metal-atom sites ($M\text{-}N_x$), where the metal atom is coordinated to multiple (usually 4) nitrogen atoms (Artyushkova et al., 2015; Chung et al., 2017; Jia et al., 2016; Zitolo

et al., 2015b) and metallic iron and/or iron carbide particles covered by N-doped graphitic carbon layers, denoted as nitrogen-doped graphitic carbon with metal (NC@M) (Ping et al., 2020; Ramaswamy & Mukerjee, 2012; Strickland et al., 2015). In addition to metal-based catalytic centers, M-N-C catalysts also feature N-C active sites. M-Nx sites generally facilitate oxygen reduction via a 4-electron pathway, whereas on NC@M and nitrogen-doped carbon (NC) sites, the ORR is thought to proceed either via a 2+2 or 2×2-electron pathway, with the underlying metal stabilizing the intermediates (Jia et al., 2015, 2016; Strickland et al., 2015).

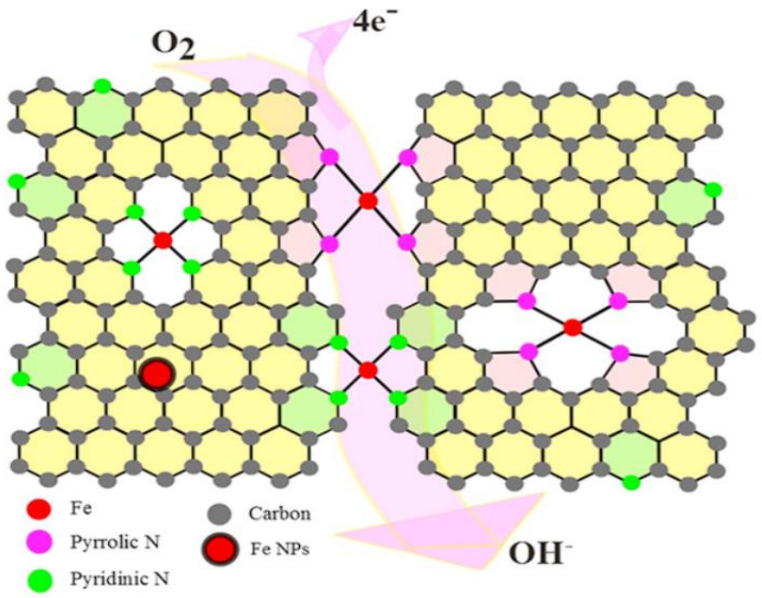

Figure 2. Different types of ORR-active sites in M-N-C catalysts (Jia et al., 2016).

The exact nature of the active sites for ORR is extremely difficult to determine due to the plurality of even this one type of active site in a given catalyst. Due to the imprecise method of synthesis (high-temperature pyrolysis), all catalysts thus far have had multiple types of active sites present. Commonly these active species are identified in a catalyst by X-ray photoelectron spectroscopy (XPS), Mössbauer spectroscopy or X-ray absorption spectroscopy (XAS). However, with all of these methods, the signal from different M-Nx sites (and in the case of XPS, also other nitrogen moieties) is overlapping and thus a large part of the identification is the deconvolution and fitting of peaks (Asset & Atanassov, 2020). In perfect systems such as graphene direct atomic-level imaging has also been achieved (Chung et al., 2017), but most of the catalysts are an amorphous mess compared to graphene and determining how many and what atoms are bound to the metal center is rather speculative with current imaging capabilities. Due to the difficulties in synthesizing a catalyst with a single type of active site, the exact reaction mechanism on this type of catalyst has also been difficult to determine.

Nonetheless, the primary objective of research into M-N-C catalysts has always been to substitute Pt catalyst on the cathode of PEMFCs. A comparison between a state-of-the-art M-N-C catalyst and a state-of-the-art Pt/C catalyst (Table 1, updated for 2019) reveals that while the activity is comparable by electrode area, the mass activity is two orders of magnitude lower. This implies that the electrode mass, and particularly the volume required to achieve the same power density as the Pt/C catalyst, will be significantly larger. In a confined space such as an automobile, increasing the electrode thickness by 100 times is clearly impractical. Moreover, thickening the electrode poses significant challenges with O_2 transport in the catalyst layer.

Table 1. Comparison of state-of-the-art Pt/C and M-N-C catalysts in PEMFCs at 0.9 V (Osmieri et al., 2021).

Catalyst	**Loading**	**Mass activity**	**Catalyst activity**
Pt/C	0.1 mg_{Pt} cm^{-2}	443 A/g_{Pt}	44.3 mA cm^{-2}
(CM-PANI)-Fe-C	6.8 mg cm^{-2}	5.2 A/g	36 mA cm^{-2}

The lower mass activity of M-N-C catalysts compared to Pt/C catalysts is due to differences in site density (SD) and turnover frequency. Studies show that Fe-N-C catalysts have significantly lower SD and turnover frequency than Pt/C catalysts (Primbs et al., 2020; Gasteiger et al., 2005; Zhou et al., 2020). Achieving comparable SD to Pt/C in M-N-C catalysts is challenging because the M-N-C sites need to be isolated and near the catalyst surface for optimal performance. Simply increasing metal content is ineffective due to metal atom agglomeration during pyrolysis. Strategies to improve SD involve segregating metal atoms using metal-organic frameworks, large ligands, or SiO_2 anchoring (Serov et al., 2015; Tian et al., 2013; H. Zhang et al., 2017; Zion et al., 2020).

1.5 Structure of carbon catalysts

PGM-free electrocatalysts offer benefits like cost-effectiveness but their lower volumetric activity remains a challenge. Numerous studies highlight the crucial role of hierarchically porous structures in carbon-based catalyst materials for boosting electrocatalytic performance (X. Wang et al., 2022). An optimal catalyst should create continuous porous channels to enhance mass transfer. Thus, the structure of the electrocatalyst support material is vital for improving fuel cell performance (Kisand et al., 2022).

Different carbon materials have been utilized for creating ORR electrocatalysts, including mesoporous carbon (R. Liu et al., 2010; Wei et al., 2014), carbon aerogels (Sarapuu et al., 2015; Wohlgemuth et al., 2012), xerogels (Fu et al., 2013), carbon nanotubes (Vikkisk et al., 2015; Yadav et al., 2015), graphene (Parvez et al., 2012; Vikkisk et al., 2014), and composite materials (Lin et al., 2012; Ma et al., 2011). These materials are highly valued for their large specific surface area, high electrical conductivity, chemical stability, and porous structure, which enhance mass transfer, active site generation, and electron transport for O_2 reduction.

Graphene, a single layer of graphite, boasts a specific surface area of 2630 $m^2\ g^{-1}$, remarkable electron mobility, thermal conductivity, and strength. However, synthesizing large quantities of single-layer graphene is difficult. Typical methods like chemical vapor deposition (CVD) and chemical exfoliation of graphite are costly and environmentally impactful (Tao et al., 2020; H. Wang et al., 2012; Peng et al., 2015; X. Liu et al., 2020). Therefore, few-layer graphene is more commonly used (Daems et al., 2014; Trogadas et al., 2014). Carbon nanotubes (CNTs) are formed by rolling sheets of graphene into tubes with sp^2 and sp^3 hybridization. They are classified into single-walled, double-walled, and multi-walled types (Iijima, 1991; Niyogi et al., 2002). CNTs are relatively easy to modify and dope but often contain metal impurities from their synthesis, which necessitates purification (Kruusenberg et al., 2011; Alexeyeva & Tammeveski, 2007). Oxidizing CNTs before doping enhances doping efficiency by forming oxygen-containing groups (Brozena et al., 2010; Shen et al., 2013). Carbide-derived carbons (CDCs) are produced by removing metal atoms from carbide lattices, resulting in a porous carbon structure. CDCs are notable for their tunable porosity and high specific surface area, making them suitable for supercapacitors and as hosts for metal-based sites (Dash et al., 2005; Jänes et al., 2009; Schmirler et al., 2011). The typical synthesis method involves thermochemical treatment in chlorine gas at high temperatures, which can be adjusted to achieve desired properties (Leis et al., 2001, 2010).

However, these carbons are mainly microporous. To attain the required porosity, synthetic methods frequently use templating techniques to form meso- and macroporous structures. This is usually done through hard-templating by using silica nanoparticles. In this method, the template remains stable at high temperatures, and the template particles are removed after pyrolysis through chemical etching, yielding carbon materials with a mesoporous structure (Pavlenko et al., 2022). However, the necessity of using concentrated HF or NaOH solutions for template removal presents a major limitation due to their toxicity, which impedes scalability and raises environmental concerns (Díez et al., 2021). A sustainable alternative to silica-based templates involves using inorganic nanoparticles such as MgO, that can be generated in-situ

during the thermal treatment (Díez et al., 2021). The primary advantage of this method is the ease of removing the templating phase, as these nanoparticles can be etched out of the carbon using dilute acid solutions, such as HCl. Inagaki et al. were pioneers in introducing a carbon preparation method utilizing this approach (Inagaki et al., 2004). A variation of the aforementioned inorganic template approach is ionothermal carbonization, which employs low-melting-point Mg salts (Jaggers et al., 2016). In this process, the carbon precursor is partially or entirely dissolved within the salt melt. Pores are generated through two mechanisms: first, the formation of nanodroplets of the molten salt that serve as a fluidic template within the carbonizing precursor; second, the development of a crosslinked carbonizing phase that encloses the in situ formed inorganic phase such as MgO nanoparticles). After heat-treatment, the template particles are removed, resulting in a porous material.

In this work, we prepare a hierarchically porous carbon support using a novel ionothermal synthesis procedure. The method uses in-situ created MgO nanoparticles to create mesopores. After carbonization under an inert atmosphere, the MgO-based template is removed using a mild HCl etching process, which is more environmentally friendly than traditional HF or NaOH leaching, used in silica-based templating. This results in a carbon material with a well-defined hierarchical porous structure, enhancing mass transfer and providing abundant active sites. To further improve electrocatalytic performance, the carbon support is doped with nitrogen and transition metals through an additional pyrolysis step. Characterization confirms the successful formation of the porous structure and uniform dopant distribution, demonstrating the material's potential for fuel cell applications.

2 THE AIMS OF THE THESIS

The primary aim of this thesis is to develop and optimize electrocatalysts for anion-exchange membrane fuel cells (AEMFCs) by focusing on the synthesis and characterization of platinum-group metal (PGM)-free catalysts for oxygen reduction reaction (ORR). This involves creating transition metal and nitrogen-doped carbon catalysts via ionothermal synthesis, conducting physical and electrochemical characterizations to evaluate their properties and performance, assessing the efficiency and stability of these PGM-free catalysts in AEMFCs compared to conventional PEMFCs with Pt-based catalysts, and optimizing the synthesis process to enhance the electrocatalytic activity and fuel cell performance.

3 METHODOLOGY

3.1. Preparation of electrocatalysts

The catalyst prepared during this work consists of three components: the carbon precursor, transition metal precursor and the nitrogen and template precursor. The carbon precursor used in this synthesis was (beta)-cyclodextrin, and template precursor was $Mg(NO_3)_2 \cdot 6H_2O$ (Alfa Aesar, 98%), the transition metal precursor was iron(II) acetate (Sigma Aldrich, 95%) and the nitrogen precursor was 1,10-phenanthroline (Thermo Scientific, 99%). The synthesis procedure can be separated into two stages: the preparation of the carbon material and doping of the carbon.

For the preparation of carbon material: (beta)-cyclodextrin and $Mg(NO_3)_2 \cdot 6H_2O$ were mixed at varying amounts with pestle and mortal (see Table 2). After ensuring homogeneity, the mixture was pyrolyzed in N_2 flow at 800 °C for 1 h, with a ramping rate of 10 °C min^{-1}. The pyrolyzed products were dispersed in 1 M HCl (Sigma-Aldrich) for 2 h at room temperature to remove the MgO template. The product was filtered and oven dried at 60 °C.

For the doping: the obtained carbon material was mixed together with iron acetate and 1,10-phenanthroline by sonication in isopropyl alcohol. The doping procedure was kept constant with a Fe-to-carbon mass ratio of 0.02. The amount of nitrogen precursor was kept at a molar ratio of 1:10 (Fe-to-phenanthroline). The mixture was oven dried and pyrolyzed again in N_2 flow at 800 °C for 1 h, with a ramping rate of 50 °C min^{-1}, to obtain the final catalysts denoted as FeNC-CDX. As a comparison the same procedure was followed by omitting the iron acetate to obtain a non-iron doped catalyst NC-CD3.

Table 2. Amounts of the precursors used in the synthesis of the catalyst materials.

Catalyst	m (β-Cyclodextrin) / g	m ($Mg(NO_3)_2 \cdot 6H_2O$) / g
FeNC-CD1	1	1
FeNC-CD2	1	0.5
FeNC-CD3	1	2
FeNC-CD4	1	3

3.2. Physical characterization

The catalyst materials were analyzed using various advanced techniques. This included scanning electron microscopy combined with energy-dispersive X-ray analysis (SEM-EDX), and transmission electron microscopy equipped with energy-dispersive X-ray analysis (STEM-

EDX) in scanning mode, utilizing both bright field (BF) and high-angle annular dark field (HAADF) detectors. Additionally, nitrogen adsorption/desorption measurements, X-ray diffraction (XRD) and X-ray photoelectron spectroscopy (XPS) were employed for thorough characterization.

The physical characterization was done in collaboration with researchers at the Institute of Chemistry, Institute of Physics, and Institute of Ecology and Earth Sciences. Dr. Jekaterina Kozlova: SEM and STEM-EDX analysis, Dr. Maike Käärik: BET with pore size distribution (PSD) analysis, Dr. Arvo Kikas: XPS analysis, Jaan Aruväli: XRD analysis.

3.3. Electrochemical measurements

A glassy carbon (GC) electrode (GC20-SS, Tokai Carbon) with a geometric surface area of 0.196 cm^2 was utilized as the working electrode. It was polished with alumina slurries of 1 and 0.3 μm (Buehler). An ultrasonically dispersed mixture containing 4 mg of the catalyst material, 960 μL of 2-propanol, and 40 μL of a 5 wt% Nafion solution in lower alcohols (Aldrich) was drop-coated onto the GC electrode. The catalyst loading on the GC electrode was 100 μg cm^{-2}. This procedure was followed to prepare electrodes coated with a commercial Pt/C catalyst (20 wt.%, E-TEK).

The rotating disk electrode (RDE) technique was used to investigate the oxygen reduction reaction (ORR) activity of the catalysts. The electrochemical measurements were carried out in a three-electrode glass cell with an Autolab potentiostat/galvanostat PGSTAT30 (Metrohm-Autolab, The Netherlands). The potential was measured against a saturated calomel electrode (SCE), and a carbon rod was used as the counter electrode. The measured values of the potentials were converted to reversible hydrogen electrode (RHE) scale as follows: $E_{RHE} = E_{SCE} + 1.008$ V. Various electrode rotation rates, from 360 to 3100 rpm, were controlled using a CTV101 speed control unit connected to an EDI101 rotator (Radiometer). The ORR measurements were performed in a 0.1 M KOH aqueous solution saturated with O_2 (99.999%, Linde). The background current was recorded in an Ar-saturated (99.999%, Linde) 0.1 M KOH solution and subtracted from the experimental O_2 reduction current. Electrochemical impedance spectroscopy (EIS) was conducted with the catalyst-coated GC electrodes in O_2-saturated 0.1 M KOH to determine the solution resistance, and iR correction was applied to the ORR polarization data using Nova 2.1 software. Durability tests involved cycling the electrode between 1.0 and 0.6 V vs RHE at a scan rate of 200 mV s^{-1}, with RDE polarization curves recorded before and after 10,000 cycles.

The RDE data was analyzed using the Koutecky-Levich (K-L) equation:

$$\frac{1}{j} = \frac{1}{j_k} + \frac{1}{j_d} = \frac{1}{j_k} - \frac{1}{0.62nFD_{O_2}^{\frac{2}{3}} v^{-\frac{1}{6}} \omega^{\frac{1}{2}} c_{O_2}^{b}} \quad (6)$$

where j is the measured current density, j_k and j_d are the kinetic and diffusion-limited current densities, respectively, n is the number of electrons transferred per O_2 molecule, F is the Faraday constant (96 485 C mol^{-1}), ω is the rotation rate (rad s^{-1}), D_{O2} is the diffusion coefficient of oxygen (1.9×10^{-5} cm^2 s^{-1}), C_{O2} is the concentration of oxygen in the bulk (1.2×10^{-6} mol cm^{-3}), and ν is the kinematic viscosity of the electrolyte solution (0.01 cm^2 s^{-1}).

3.4 AEMFC tests

For the anodes, ~22 mg of powdered anion-exchange ionomer (Fumion®, Fumatech) was ground in a mortar for 3 min, after which 61 mg of PtRu/C catalyst (40% Pt and 20% Ru on carbon black HiSPEC 10000, Alfa Aesar) was added to the mortar along with 30 mg of carbon black (Vulcan XC-72) to increase the porosity and hydrophobicity of the catalyst layer and thereby avoid flooding. After that, 1 mL of deionized water and 9 mL of 2-propanol were added to the mortar and further ground for 10 min, to obtain a low-viscosity catalyst ink. The cathode catalyst ink of FeNC-CD3 was prepared by grinding 13 mg of ionomer, then adding 20 mg of catalyst and 10 mL of total solvents and grinding for an additional 10 min.

The catalyst inks were sonicated for 1 h in an ice-cooled ultrasonic bath (Grant XUBA3) at 100% intensity. After sonication, the cathode inks were sprayed onto 2.25 cm^2 Toray Carbon Paper 060 gas diffusion layers (GDLs), using an Iwata HP-TH professional airbrush. The loading of the cathode catalyst on GDE was 0.9 mg cm^{-2}. The anode ink was spray-deposited onto a 6.05 cm^2 Toray Carbon Paper 060 GDL with 5% wet-proofing up to the loading of 0.75 mg_{PtRu} cm^{-2}, after which two smaller 2.25 cm^2 GDEs were cut from it.

For cell assembly two 5 cm^2 a piece of FAA-3-05-RF polymer reinforced anion-exchange membrane (AEM) with porous ePTFE-film, 7 μm average fully hydrated thickness (Fumatech) and all electrodes were immersed in 1 M KOH aqueous solution for 1 h, while changing the solution every 20 min. Two different MEAs were assembled between two 5 cm^2 single-serpentine graphite bipolar flow field plates with Teflon gaskets and torqued to 4.5 N m to achieve an average GDL compression of 30%. The AEMFC tests were carried out in an 850E Scribner Associates Fuel Cell test station under H_2/O_2 gas (99.999%) at cell temperatures of 80 °C with 100 kPa of back-pressurisation.

The MEA preparation and AEMFC measurements were done in collaboration with John C. Douglin at Technion – Israel Institute of Technology.

4 RESULTS AND DISCUSSION

4.1 Physical characterization

$Mg(NO_3)_2 \cdot 6H_2O$ was selected as the precursor because of its low melting point (88.9 °C), which is below the carbonization temperature of β-cyclodextrin, making it the ideal ionothermal liquid reaction medium. The nitrogen-containing precursor was specifically chosen to simultaneously introduce nitrogen moieties into the carbonizing phase. During the heat-treatment process, cyclodextrin is partially dissolved in the molten salt and the pore formation occurs through two primary mechanisms. First, as the temperature increases the larger pores are generated by the liquid salt droplets within the carbonizing phase. Next, the in-situ formed MgO nanoparticles are partially covered by the carbonizing phase and a composite material consisting of MgO nanoparticles and N-doped carbon (MgO@NC) is obtained (Pampel et al., 2016)**.** The smaller mesopores are formed after the acid-treatment procedure when the MgO nanoparticles (the sacrificial-template) are washed out by dispersing the material in 1 M HCl (Menga et al., 2019). The acid-treated material is then mixed with iron acetate and 1,10-phenanthroline and pyrolyzed again, to introduce the ORR-active sites. The scanning electron microscopy (SEM) images reveal a hierarchically porous structure (Fig. 3) that includes both macropores and larger mesopores. A closer magnification (Fig. 3c) reveals the numerous small mesopores left in the carbon structure after the removal of the MgO template. The SEM-EDX analysis does not reveal any Mg left in the material after the acid-treatment procedure and subsequent Fe-doping, however around 5 wt.% of Fe and 6 wt.% of N can be detected.

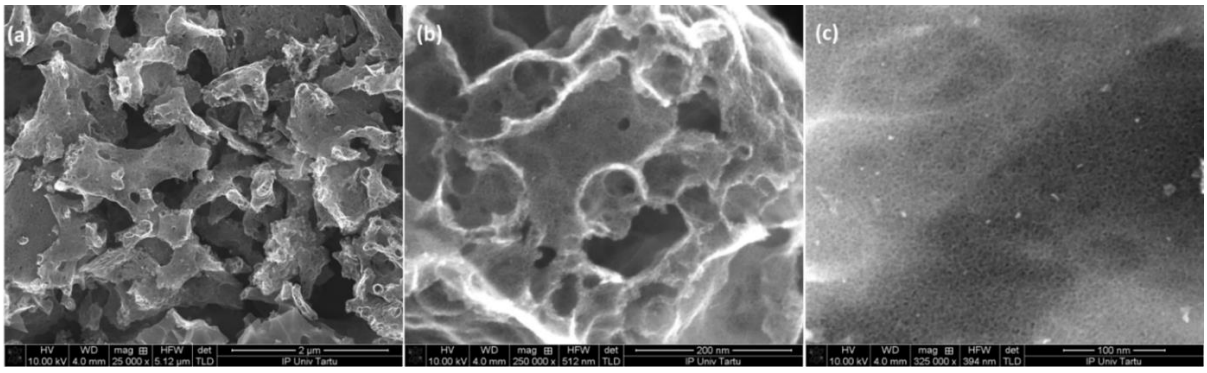

Figure 3. SEM images of FeNC-CD3 at different magnifications displaying the hierarchical porosity (a, b) and the small mesopores created by the sacrificial-template (c).

The effective removal of MgO nanoparticles can be further confirmed by the powder X-ray diffraction (XRD) measurements (Fig. 4b). The non-acid treated material MgO@NC-CD3 displays prominent peaks indexed to MgO phase (PDF-00-045-0946) with an average

crystallite size of around 4 nm, this phase does not appear in the final catalyst FeNC-CD3. However additional peaks indexed to metallic Fe (PDF-04-002-3692) and Fe-carbide (PDF-00-034-0001) have appeared after the doping procedure.

Figure 4a presents the pore size distribution (PSD) graph and N_2 adsorption-desorption isotherms of different catalysts. The isotherms exhibit a steep increase at low pressure, signifying the presence of some microporosity in the carbon materials. This microporosity is attributed to the rapid release of gases during the nitrate-salt decomposition. The slope at higher relative pressures indicates the filling of mesopores. The PSD graph displays prominent peaks at around 5 nm for all materials (Fig. 4a). These pores are created when the MgO nanoparticles are removed during the acid-treatment. Exact information about the larger pores cannot be obtained due to the limit-of-detection for N_2 adsorption-desorption measurements, however their presence is confirmed by both SEM and High-Angle Annular Dark-Field Scanning Transmission Electron Microscopy (HAADF-STEM) images. The FeNC-CD3 material displays a relatively high specific surface area specific differential function theory (S_{DFT}) of 817 $m^2\ g^{-1}$. Unsurprisingly, the FeNC-CD1 material displays a much lower S_{DFT} of 412 $m^2\ g^{-1}$, since the amount of $Mg(NO_3)_2$ precursor used in the synthesis was smaller (see Table 2). Interestingly, if the amount of $Mg(NO_3)_2$ is further increased (FeNC-CD4) the S_{DFT} is lowered to 666 $m^2\ g^{-1}$. This can likely be attributed to the collapse of the carbon structure due to an excess of the templating phase.

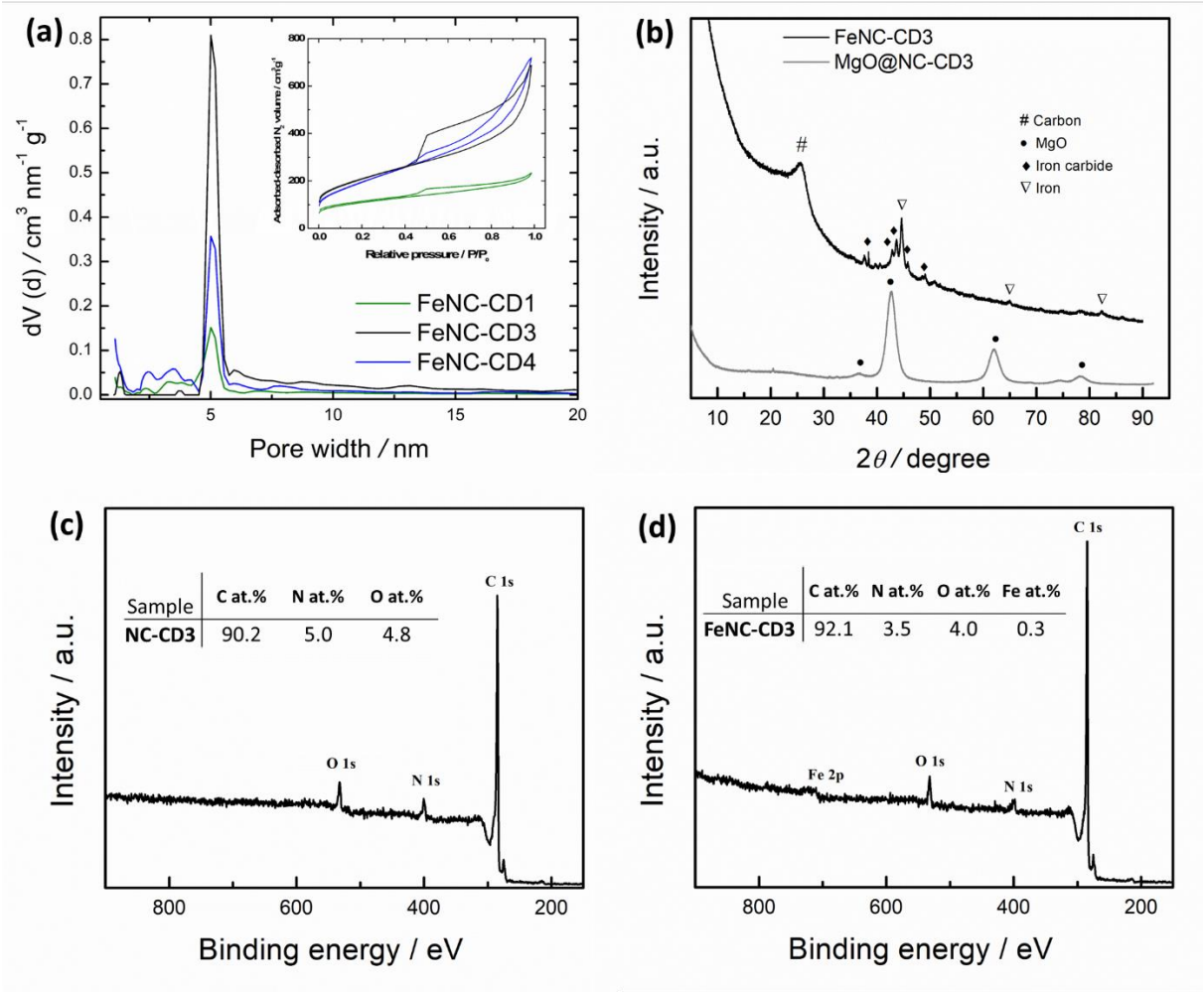

Figure 4. (a) Pore size distribution of the prepared catalysts, with the inset displaying the N_2 adsorption-desorption isotherms, (b) XRD patterns of the final catalyst and non-acid washed MgO@NC-CD3 material, (c, d) XPS survey spectra of NC-CD3 and FeNC-CD3 with the insets showing the respective elemental compositions in atomic percentage.

The high-angle annular dark-field scanning transmission electron microscopy (HAADF-STEM) images (Fig. 5) similarly reveal a hierarchically porous carbon structure, with both macropores and mesopores. The presence of mesopores is crucial for several reasons. Mesopores, with their intermediate size, provide a large surface area that facilitates enhanced interactions between the carbon material and the catalytic sites, improving the overall efficiency of the material. They also enable better mass transport of reactants and products within the structure, which is essential for applications such as fuel cells and batteries (X. Wang et al., 2022). Additionally, numerous spherical metallic nanoparticles that are created during the carbon doping procedure can be seen. Some of the nanoparticles are larger in size, however smaller nanoparticles can also be detected. The HAADF STEM images of FeNC-CD3 along with the overlays of Energy-Dispersive X-ray Spectroscopy (EDX) maps for Fe and N

elements, display an even distribution of both Fe and N throughout the carbon material, along with agglomerated iron-containing nanoparticles. These particles are most likely both metallic iron and iron carbide as these phases were detected in XRD measurements. The bright-field (BF) images (Fig. 6d and e) reveal a layered graphitic structure in some locations; in some cases, the nanoparticles are surrounded by these layers. Increased graphitization of the carbon structure increases the electronic conductivity of the material, as well as helping prevent significant carbon corrosion during FC operation.

The pyrolysis temperature used in the preparation of these materials was 800 °C, too low for significant graphitization to occur as graphitization generally begins at above 1300 °C. However, it is well established that iron can catalyze graphitization at lower temperatures (Menga et al., 2021). During the second pyrolysis at elevated temperatures, the iron acetate precursor is reduced, and iron nanoparticles are created. Metallic iron can then be further reduced through carbothermal reduction, forming iron carbide, and allowing for dissociative reaction mechanisms that essentially recrystallize the carbon structure causing the graphitization of the carbon and at the same time the loss of heteroatoms (Menga et al., 2021). This is evidenced by the XRD patterns for FeNC-CD3 (Fig. 4b), where peaks corresponding to these two phases appear.

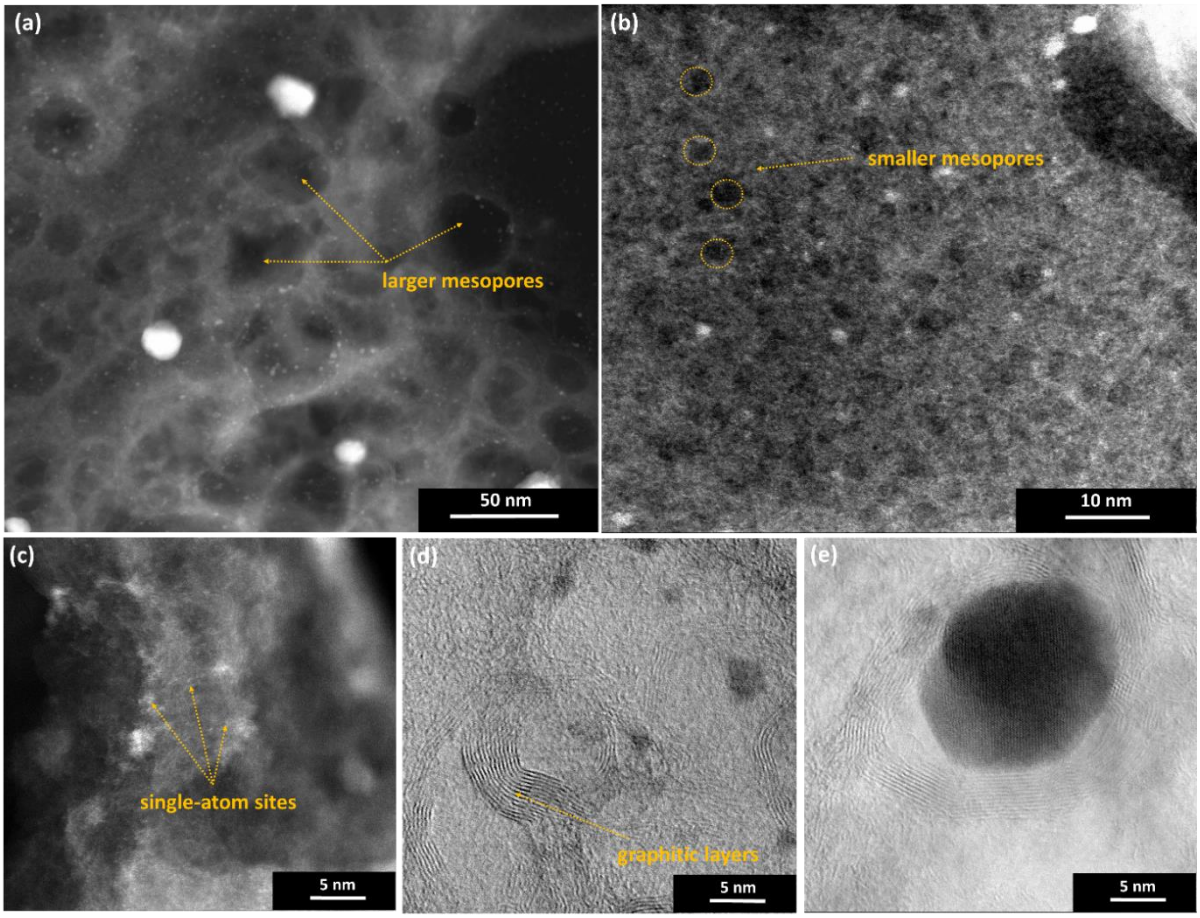

Figure 5. (a, b, c) HAADF-TEM images of FeNC-CD3 showing the macro- and mesoporosity, agglomerated iron particles and single-atom Fe sites, respectively. (d, e) BF images showing the graphitic domains and an iron-containing nanoparticle surrounded by layers of graphitic carbon.

The XPS survey spectra display peaks at 285, 400, and 532 eV, corresponding to binding energies of C 1s, N 1s, and O 1s (Figs. 4c and d). Additionally, for FeNC-CD3 catalyst a small Fe peak at 711 eV is detected after the doping. The loss of heteroatoms can be seen when comparing the XPS spectra of NC-CD3 and the iron-doped FeNC-CD3 materials, where a reduction in both N and O signals can be observed, despite the inclusion of additional N-precursor (1,10-phenanthroline). At the same time, the C 1s high-resolution XPS spectra (and Figs. 7a and c) display an increase in the carbide peak as well as the sp2 carbon peak for FeNC-CD3 catalyst, indicating increased graphitization of the carbon structure after the Fe-doping procedure. This is further evidenced by the XRD patterns, where the MgO@NC-CD3 does not display a prominent peak at 25º, consisting primarily of amorphous carbon material, however after the doping procedure a graphitic carbon phase appears (PDF-01-077-7164). At the same time additional pyridinic N sites are formed, as can be seen from in high-resolution XPS N 1s

spectra (Figs. 7b and d) comparing FeNC-CD3 to NC-CD3, where the pyridinic form of N is noticeably increased for FeNC-CD3. This mechanism has also been observed in other works (Menga et al., 2021**;** Koyuturk et al., 2022). Interestingly, M-N_x sites are present even in the undoped NC-CD3 material (see Fig. 7b). These are likely pyrrolic Mg-N_x sites, as previous works by both our workgroup as well as other research groups have noted that Mg-N_x sites are formed if both Mg and N sources are present during pyrolysis (Kisand et al., 2022 ;Koyuturk et al., 2022). Surprisingly, no Mg can be observed in FeNC-CD3 material (according to EDX analysis, see Fig. 8), we propose that the Mg atoms in the M-N_x sites are replaced with Fe during the second pyrolysis, as it has been observed that metallic iron nanoparticles can decompose and release Fe atoms during the heat-treatment that can then coordinate with nitrogen moieties and in this case also with Mg-N_x sites. The existence of atomically dispersed Fe-N_x sites can be seen in FeNC-CD3 material (Fig. 5c and Fig. 6c and d), but it is not possible to differentiate between the pyridinic and pyrrolic varieties in these images. In summary, we propose that the mechanism of the formation of Fe-N_x sites can be separated into two processes. Firstly, some of the generated pyridinic sites will coordinate with the released Fe atoms forming pyridinic M-N_x sites. Secondly, some of the Fe atoms will replace Mg in the pyrrolic Mg-N_x sites. Although, this proposed mechanism requires further research to confirm.

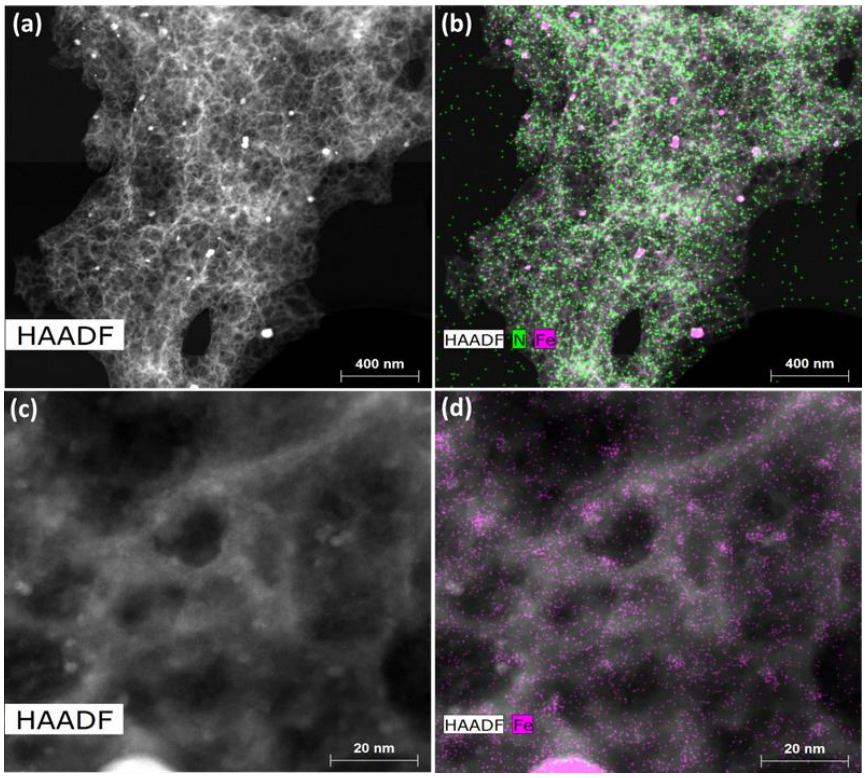

Figure 6. (a, c) HAADF-STEM images of FeNC-CD3 and (b, d) the overlays of EDX maps of the Fe and N elements.

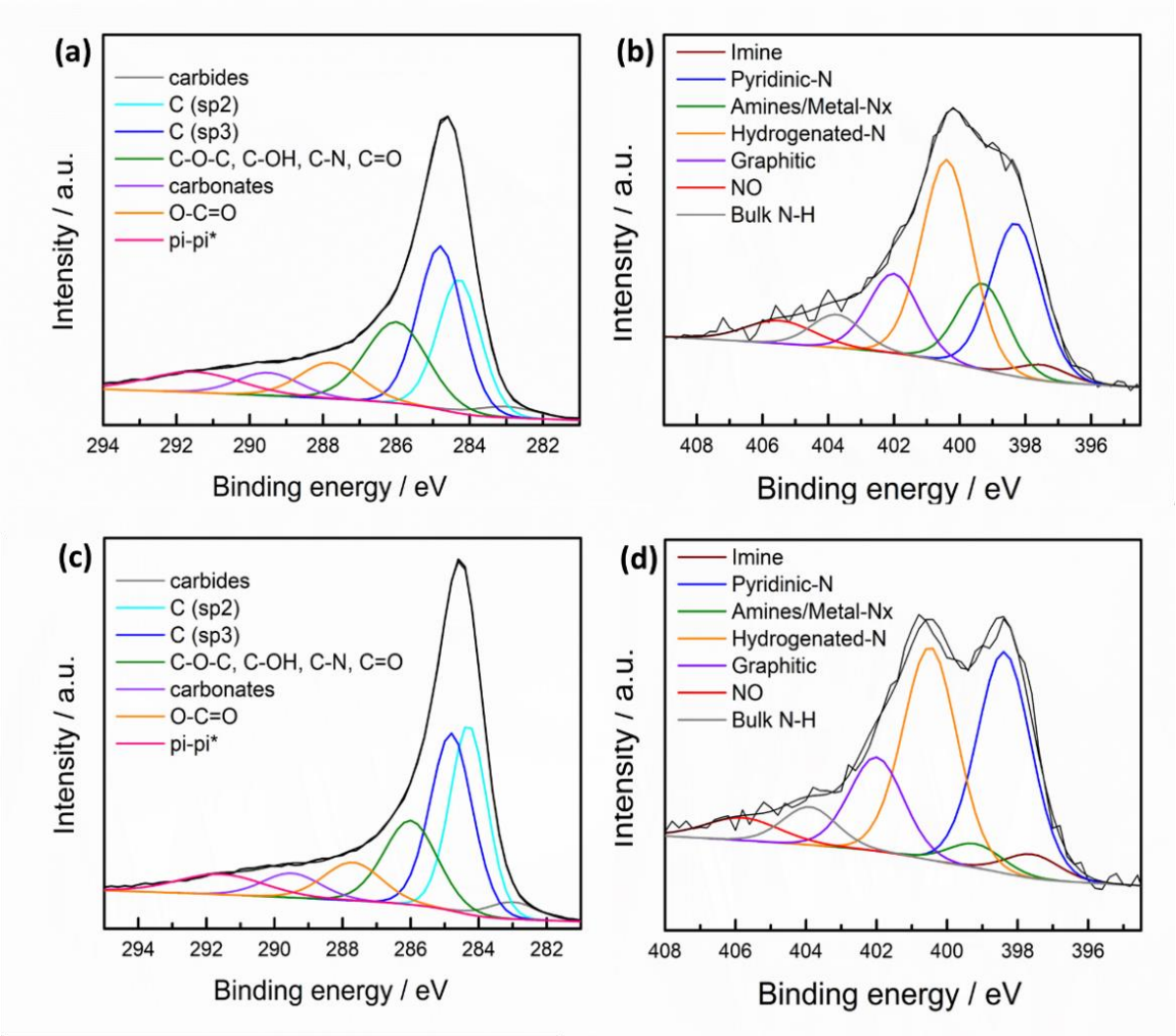

Figure 7. (a, c) XPS high-resolution C 1s spectra for NC-CD3 and FeNC-CD3, respectively and (b, d) XPS high-resolution N 1s spectra for NC-CD3 and FeNC-CD3, respectively.

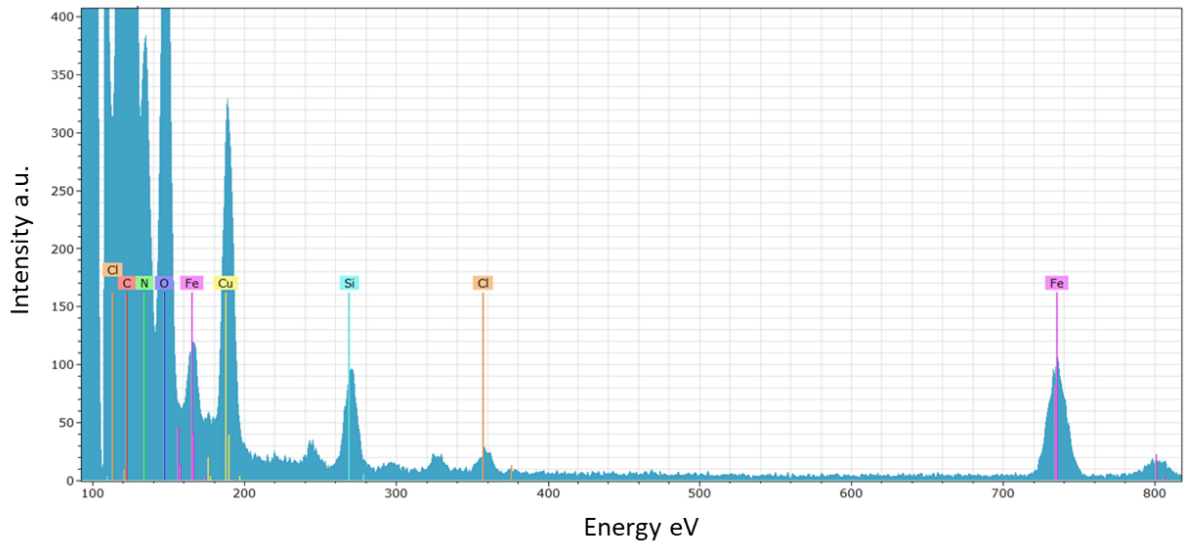

Figure 8. STEM-EDX spectra for FeNC-CD3.

4.2 Electrochemical characterization

Rotating disc electrode (RDE) measurements were employed to conduct the preliminary assessment of the electrocatalytic performance of the nanocarbon-based catalysts for the ORR in 0.1 M KOH electrolyte. The linear sweep voltammograms (LSVs) of the different catalysts were analyzed (Fig. 7). As metal-free electrocatalysts usually display a poorer electrocatalytic activity, unsurprisingly the NC-CD3 catalyst showed low ORR activity, as can be seen from the more negative onset (E_{onset}) and half-wave potential ($E_{1/2}$) values, indicating a large overpotential for ORR (see Table 3). After the Fe-doping the electrocatalytic activity is significantly increased, characterized by more positive E_{onset} and $E_{1/2}$ values. We additionally set out to optimize the organic precursor to templating precursor ratio, while keeping the doping procedure constant. Comparing the catalysts with each other (Table 2), it is evident that 1:2 mass ratio of cyclodextrin to Mg-nitrate (corresponding to FeNC-CD3) displays the highest E_{onset} and $E_{1/2}$ values, even surpassing the commercial Pt/C catalyst. The excellent electrocatalytic activity is attributed to the high-density of both pyrrolic and pyridinic Fe-N_x sites, created through the ionothermal synthesis method. Additionally, Fe@N-C sites have been shown to also be ORR active in alkaline media and can further boost the ORR activity (Hu et al., 2014) and such sites are presents in our catalyst materials according to both STEM and XRD analysis.

The difference of ORR activity between the prepared FeNC-CD catalysts can be in part explained by the carbon nanostructure. The S_{DFT} value correlates quite well with electrocatalytic activity. Higher mesoporous specific surface area helps to expose more active sites to the electrolyte, thus increasing the electrocatalytic activity (Kisand et al., 2022). FeNC-CD1 material displayed the lowest S_{DFT} value and also a comparatively lower electrocatalytic activity. FeNC-CD4 has a increased surface area and better ORR activity, while FeNC-CD3 displays the highest S_{DFT} value and electrocatalytic performance. However, this huge difference in performance between the catalysts cannot be explained by only the $S_{DFT.}$. It can be assumed that the ratio of cyclodextrin-to-$Mg(NO_3)_2$ likely affects the site density (SD) of the materials in addition to the carbon structure.

Table 3. E_{onset}, $E_{1/2}$ and n values (obtained from K-L analysis) of various catalysts in 0.1 M KOH.

Catalyst	E_{onset} **/ V**	$E_{1/2}$ **/ V**	n **(at 0.6 V)**
NC-CD3	0.86	0.79	3.1
FeNC-CD1	0.95	0.81	4.4
FeNC-CD2	0.93	0.80	4.1
FeNC-CD3	0.98	0.90	4.0
FeNC-CD4	0.96	0.88	4.2

To investigate the kinetics of the ORR in greater detail, LSV curves were measured at various rotation rates ranging from 360 to 3100 rpm (Fig. 7c). The results showed distinct limiting current plateaus and a consistent onset potential. The K-L plots (Fig. 6d) demonstrated a good linearity, implying first-order reaction kinetics, as well as a consistent *n* value (calculated from the K-L slopes) of 4 in a wide potential range. In addition, for NC-CD3 the value of *n* is around 3, commonly observed for N-doped carbon-based catalysts (Q. Li et al., 2017). These results are highly favorable for several reasons. Firstly, the good linearity of the K-L plots and the consistent *n* value of 4 indicate efficient electrocatalytic activity and reliable reaction kinetics. The *n* value close to 4 suggests that the catalysts facilitate a more complete reduction of O_2 to water, which is the most desired pathway in ORR for fuel cells, as it maximizes energy output and minimizes the formation of undesirable byproducts like hydrogen peroxide (Ratso, 2020). The distinct limiting current plateaus and consistent onset potential observed in the LSV curves further confirm the catalysts' effectiveness, which is crucial for practical applications.

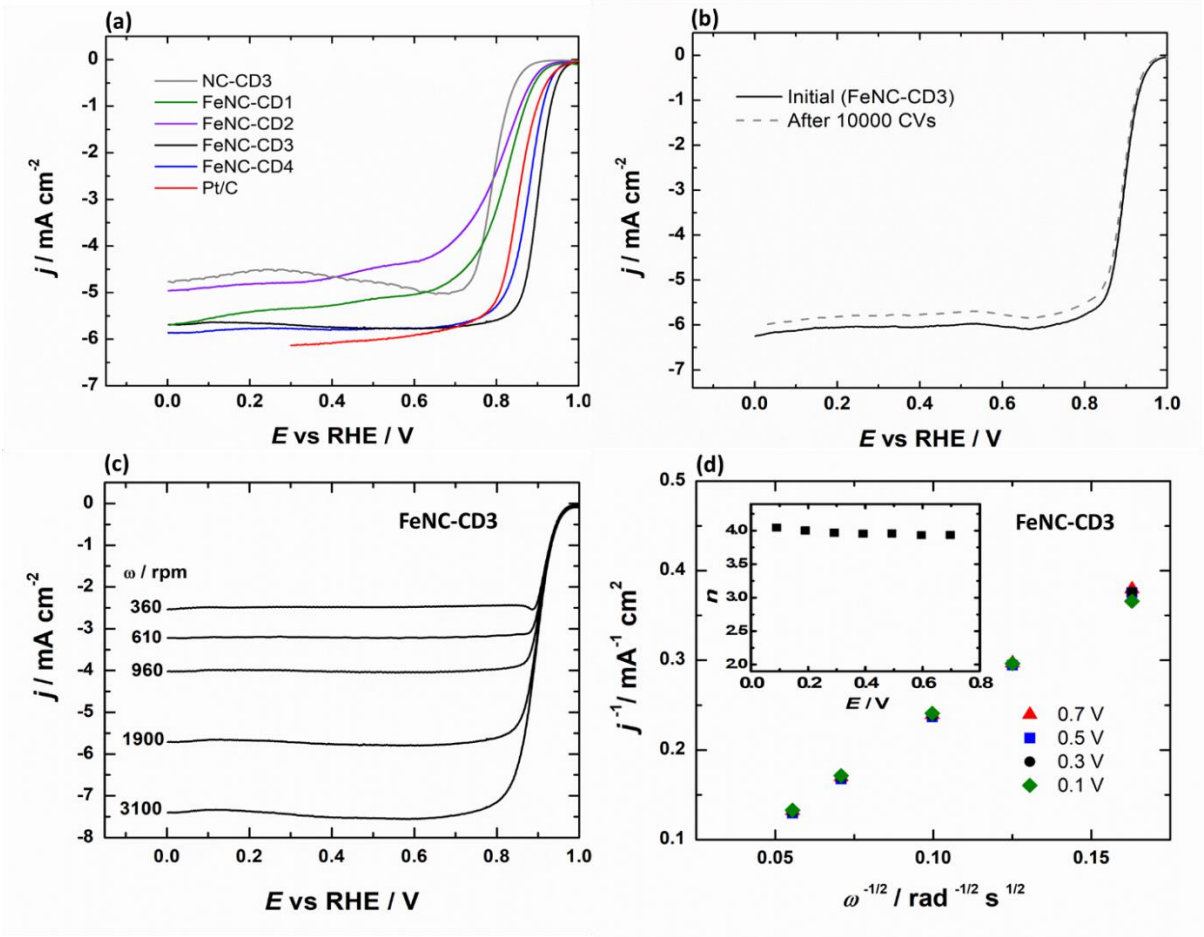

Figure 9. (a) Comparison of RDE voltammetry curves for ORR on various electrocatalysts in O_2-saturated 0.1 M KOH solution at 1900 rpm; (b) RDE voltammetry curves for O_2 reduction before and after repetitive potential cycles for the FeNC-CD3 catalyst; (c) RDE voltammetry curves for oxygen reduction in O_2-saturated 0.1 M KOH solution at different rotation rates for FeNC-LT and (d) K-L plots derived from the RDE data with the inset showing the number of electrons transferred per O_2 molecule.

The accelerated stability test of FeNC-CD3 was performed by continuous potential cycling in O_2-saturated 0.1 M KOH, between 1.0 and 0.6 V vs RHE, at a scan rate of 200 mV s^{-1} (Fig. 9b). After 10,000 cycles, the ORR electrocatalytic activity showed only a slight decrease in the $E_{1/2}$ value of 2.4 mV, demonstrating excellent stability in RDE tests, which is attributed to the well graphitized carbon structure.

The FeNC-CD3 catalyst underwent additional testing in single-cell AEMFC measurements, where it demonstrated moderate fuel cell performance as the cathode catalyst, achieving a peak power density (P_{max}) of 596 mW cm^{-2} (Fig. 10a). Compared to the thin catalyst layers and high SD of PGM-based catalysts, the FeNC-CD3 catalyst has a much lower volumetric activity

resulting in the need for a significantly thicker catalyst layer. This in turn causes a higher area specific resistance (ASR) and lowers the performance of the fuel cell. As such, even though the catalyst displayed greater electrocatalytic activity in RDE measurements compared to the Pt/C catalyst, the best performance obtained with Pt/C cathode in AEMFC is still significantly higher at P_{max} of 3.4 W cm^{-2} (Ul Hassan et al., 2020). However, since AEMFC performance is significantly influenced by the test conditions and most importantly MEA manufacturing techniques and other MEA components, such as the AEM and ionomer (Firouzjaie & Mustain, 2020), the results obtained by different research groups cannot be directly compared.

It is well known that the thicker catalyst layer for PGM-free catalysts can cause flooding issues within the cell, especially at higher current densities (Firouzjaie & Mustain, 2020). The hierarchical porosity can somewhat alleviate this concern, and as can be seen from the polarization curve (Fig. 10a), no significant flooding issues can be observed at the optimized dew points for FeNC-CD3 cathode.

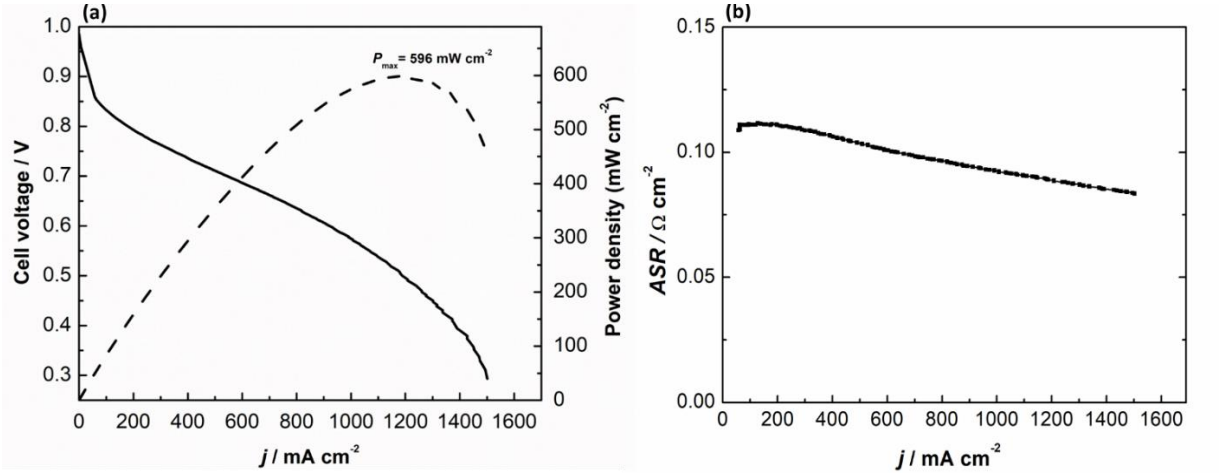

Figure 10. H_2-O_2 (flow rates of 1 and 0.74 L min^{-1}) AEMFC performance of FeNC-CD3 cathode catalyst loaded to 0.9 mg cm^{-2} with an applied backpressure of 100 kPa on both anode and cathode compartments. (a) Polarization and power density curves and (b) corresponding Area specific resistance values (ASR) versus current density.

SUMMARY

This thesis explores the development of PGM-free catalysts for AEMFC application, addressing the limitations associated with the high cost and scarcity of platinum. By synthesizing transition metal and nitrogen-doped carbon-based catalysts with mesoporous structure, the study aims to provide an efficient and sustainable alternative to traditional Pt/C catalysts. The physical and electrochemical characterizations of these catalysts revealed promising features such as highly mesoporous structure and well-distributed active sites, which are crucial for enhancing electrocatalytic activity.

Electrochemical tests, including rotating disk electrode measurements, demonstrated that the optimized catalysts exhibit excellent oxygen reduction reaction activity, with high onset potentials and favorable Koutecky-Levich plot linearity. These findings indicate efficient electrocatalytic behavior and reliable reaction kinetics. The stability tests showed that the catalysts maintain their performance by repetitive potential cycling, further confirming their suitability for practical applications.

The results highlight that the newly developed FeNC-CD3 catalyst outperforms traditional Pt/C catalysts in RDE tests, making it a strong candidate for AEMFC cathodes. Despite the challenges associated with achieving high site densities and avoiding metal agglomeration, the study provides valuable insights into the synthesis and optimization processes, paving the way for future advancements in fuel cell technology. This research contributes to the broader goal of developing cost-effective and sustainable energy solutions, aligning with global efforts to reduce carbon dioxide emissions and transition towards cleaner energy sources.

REFERENCES

Alexeyeva, N., & Tammeveski, K. (2007). Electrochemical Reduction of Oxygen on Multiwalled Carbon Nanotube Modified Glassy Carbon Electrodes in Acid Media. *Electrochemical and Solid-State Letters*, *10*(5), F18. https://doi.org/10.1149/1.2713657

Artyushkova, K., Serov, A., Rojas-Carbonell, S., & Atanassov, P. (2015). Chemistry of Multitudinous Active Sites for Oxygen Reduction Reaction in Transition Metal–Nitrogen–Carbon Electrocatalysts. *The Journal of Physical Chemistry C*, *119*(46), 25917–25928. https://doi.org/10.1021/acs.jpcc.5b07653

Asset, T., & Atanassov, P. (2020). Iron-Nitrogen-Carbon Catalysts for Proton Exchange Membrane Fuel Cells. *Joule*, *4*(1), 33–44. https://doi.org/10.1016/j.joule.2019.12.002

Banham, D., Choi, J., Kishimoto, T., & Ye, S. (2019). Integrating PGM-Free Catalysts into Catalyst Layers and Proton Exchange Membrane Fuel Cell Devices. *Advanced Materials*, *31*(31), 1804846. https://doi.org/10.1002/adma.201804846

Banham, D., Kishimoto, T., Zhou, Y., Sato, T., Bai, K., Ozaki, J., Imashiro, Y., & Ye, S. (2018). Critical advancements in achieving high power and stable nonprecious metal catalyst–based MEAs for real-world proton exchange membrane fuel cell applications. *Science Advances*, *4*(3), eaar7180. https://doi.org/10.1126/sciadv.aar7180

Banham, D., & Ye, S. (2017). Current Status and Future Development of Catalyst Materials and Catalyst Layers for Proton Exchange Membrane Fuel Cells: An Industrial Perspective. *ACS Energy Letters*, *2*(3), 629–638. https://doi.org/10.1021/acsenergylett.6b00644

Bashyam, R., & Zelenay, P. (2006). A class of non-precious metal composite catalysts for fuel cells. *Nature*, *443*(7107), 63–66. https://doi.org/10.1038/nature05118

Brozena, A. H., Moskowitz, J., Shao, B., Deng, S., Liao, H., Gaskell, K. J., & Wang, Y. (2010). Outer Wall Selectively Oxidized, Water-Soluble Double-Walled Carbon Nanotubes. *Journal of the American Chemical Society*, *132*(11), 3932–3938. https://doi.org/10.1021/ja910626u

Byon, H. R., Suntivich, J., Crumlin, E. J., & Shao-Horn, Y. (2011). Fe–N-modified multi-walled carbon nanotubes for oxygen reduction reaction in acid. *Physical Chemistry Chemical Physics*, *13*(48), 21437. https://doi.org/10.1039/c1cp23029h

Carvalho, A. C. M., & Dos Santos, M. C. (2006). Nitrogen-substituted nanotubes and nanojunctions: Conformation and electronic properties. *Journal of Applied Physics*, *100*(8), 084305. https://doi.org/10.1063/1.2357646

Chenitz, R., Kramm, U. I., Lefèvre, M., Glibin, V., Zhang, G., Sun, S., & Dodelet, J.-P. (2018). A specific demetalation of Fe–N4 catalytic sites in the micropores of NC_Ar + NH3 is at the origin of the initial activity loss of the highly active Fe/N/C catalyst used for the reduction of oxygen in PEM fuel cells. *Energy & Environmental Science*, *11*(2), 365–382. https://doi.org/10.1039/C7EE02302B

Choi, C. H., Lim, H.-K., Chung, M. W., Chon, G., Sahraie, N. R., Altin, A., Sougrati, M.-T., Stievano, L., Oh, H. S., Park, E. S., Luo, F., Strasser, P., Dražić, G., Mayrhofer, K. J. J., Kim, H., & Jaouen, F. (2018). The Achilles' heel of iron-based catalysts during oxygen reduction in an acidic medium. *Energy & Environmental Science*, *11*(11), 3176–3182. https://doi.org/10.1039/C8EE01855C

Chung, H. T., Cullen, D. A., Higgins, D., Sneed, B. T., Holby, E. F., More, K. L., & Zelenay, P. (2017). Direct atomic-level insight into the active sites of a high-performance PGM-free ORR catalyst. *Science*, *357*(6350), 479–484. https://doi.org/10.1126/science.aan2255

Czerw, R., Terrones, M., Charlier, J.-C., Blase, X., Foley, B., Kamalakaran, R., Grobert, N., Terrones, H., Tekleab, D., Ajayan, P. M., Blau, W., Rühle, M., & Carroll, D. L. (2001). Identification of Electron Donor States in N-Doped Carbon Nanotubes. *Nano Letters*, *1*(9), 457–460. https://doi.org/10.1021/nl015549q

Daems, N., Sheng, X., Vankelecom, I. F. J., & Pescarmona, P. P. (2014). Metal-free doped carbon materials as electrocatalysts for the oxygen reduction reaction. *Journal of Materials Chemistry A*, *2*(12), 4085–4110. https://doi.org/10.1039/C3TA14043A

Dai, L., Xue, Y., Qu, L., Choi, H.-J., & Baek, J.-B. (2015). Metal-Free Catalysts for Oxygen Reduction Reaction. *Chemical Reviews*, *115*(11), 4823–4892. https://doi.org/10.1021/cr5003563

Dash, R. K., Yushin, G., & Gogotsi, Y. (2005). Synthesis, structure and porosity analysis of microporous and mesoporous carbon derived from zirconium carbide. *Microporous and Mesoporous Materials*, *86*(1–3), 50–57. https://doi.org/10.1016/j.micromeso.2005.05.047

Dekel, D. R. (2018). Review of cell performance in anion exchange membrane fuel cells. *Journal of Power Sources*, *375*, 158–169. https://doi.org/10.1016/j.jpowsour.2017.07.117

Díez, N., Sevilla, M., & Fuertes, A. B. (2021). Synthesis strategies of templated porous carbons beyond the silica nanocasting technique. *Carbon*, *178*, 451–476. https://doi.org/10.1016/j.carbon.2021.03.029

Domínguez, C., Pérez-Alonso, F. J., Abdel Salam, M., Al-Thabaiti, S. A., Obaid, A. Y., Alshehri, A. A., Gómez De La Fuente, J. L., Fierro, J. L. G., & Rojas, S. (2015). On the relationship between N content, textural properties and catalytic performance for the oxygen reduction reaction of N/CNT. *Applied Catalysis B: Environmental*, *162*, 420–429. https://doi.org/10.1016/j.apcatb.2014.07.002

Ferrandon, M., Kropf, A. J., Myers, D. J., Artyushkova, K., Kramm, U., Bogdanoff, P., Wu, G., Johnston, C. M., & Zelenay, P. (2012). Multitechnique Characterization of a Polyaniline–Iron–Carbon Oxygen Reduction Catalyst. *The Journal of Physical Chemistry C*, *116*(30), 16001–16013. https://doi.org/10.1021/jp302396g

Ferre-Vilaplana, A., & Herrero, E. (2019). Why nitrogen favors oxygen reduction on graphitic materials. *Sustainable Energy & Fuels*, *3*(9), 2391–2398. https://doi.org/10.1039/C9SE00262F

Firouzjaie, H. A., & Mustain, W. E. (2020). Catalytic Advantages, Challenges, and Priorities in Alkaline Membrane Fuel Cells. *ACS Catalysis*, *10*(1), 225–234. https://doi.org/10.1021/acscatal.9b03892

Fu, X., Jin, J., Liu, Y., Liu, Q., Niu, K., Zhang, J., & Cao, X. (2013). Graphene-xerogel-based non-precious metal catalyst for oxygen reduction reaction. *Electrochemistry Communications*, *28*, 5–8. https://doi.org/10.1016/j.elecom.2012.11.017

Gasteiger, H. A., Kocha, S. S., Sompalli, B., & Wagner, F. T. (2005). Activity benchmarks and requirements for Pt, Pt-alloy, and non-Pt oxygen reduction catalysts for PEMFCs. *Applied Catalysis B: Environmental*, *56*(1), 9–35. https://doi.org/10.1016/j.apcatb.2004.06.021

Goellner, V., Armel, V., Zitolo, A., Fonda, E., & Jaouen, F. (2015). Degradation by Hydrogen Peroxide of Metal-Nitrogen-Carbon Catalysts for Oxygen Reduction. *Journal of The Electrochemical Society*, *162*, H403–H414. https://doi.org/10.1149/2.1091506jes

Gottesfeld, S., Dekel, D. R., Page, M., Bae, C., Yan, Y., Zelenay, P., & Kim, Y. S. (2018). Anion exchange membrane fuel cells: Current status and remaining challenges. *Journal of Power Sources*, *375*, 170–184. https://doi.org/10.1016/j.jpowsour.2017.08.010

G. Santori, P., N. Mondal, A., R. Dekel, D., & Jaouen, F. (2020). The critical importance of ionomers on the electrochemical activity of platinum and platinum-free catalysts for anion-exchange membrane fuel cells. *Sustainable Energy & Fuels*, *4*(7), 3300–3307. https://doi.org/10.1039/D0SE00483A

Guo, D., Shibuya, R., Akiba, C., Saji, S., Kondo, T., & Nakamura, J. (2016). Active sites of nitrogen-doped carbon materials for oxygen reduction reaction clarified using model catalysts. *Science*, *351*(6271), 361–365. https://doi.org/10.1126/science.aad0832

Guo, J., Hsu, A., Chu, D., & Chen, R. (2010). Improving Oxygen Reduction Reaction Activities on Carbon-Supported Ag Nanoparticles in Alkaline Solutions. *The Journal of Physical Chemistry C*, *114*(10), 4324–4330. https://doi.org/10.1021/jp910790u

Gupta, S., Tryk, D., Bae, I., Aldred, W., & Yeager, E. (1989). Heat-treated polyacrylonitrile-based catalysts for oxygen electroreduction. *Journal of Applied Electrochemistry*, *19*(1), 19–27. https://doi.org/10.1007/BF01039385

He, Q., & Cairns, E. J. (2015). Review—Recent Progress in Electrocatalysts for Oxygen Reduction Suitable for Alkaline Anion Exchange Membrane Fuel Cells. *Journal of The Electrochemical Society*, *162*(14), F1504. https://doi.org/10.1149/2.0551514jes

He, Q., Yang, X., He, R., Bueno-López, A., Miller, H., Ren, X., Yang, W., & Koel, B. E. (2012). Electrochemical and spectroscopic study of novel Cu and Fe-based catalysts for oxygen reduction in alkaline media. *Journal of Power Sources*, *213*, 169–179. https://doi.org/10.1016/j.jpowsour.2012.04.029

Herranz, J., Jaouen, F., Lefèvre, M., Kramm, U. I., Proietti, E., Dodelet, J.-P., Bogdanoff, P., Fiechter, S., Abs-Wurmbach, I., Bertrand, P., Arruda, T. M., & Mukerjee, S. (2011). Unveiling N-Protonation and Anion-Binding Effects on Fe/N/C Catalysts for O2 Reduction in Proton-Exchange-Membrane Fuel Cells. *The Journal of Physical Chemistry C*, *115*(32), 16087–16097. https://doi.org/10.1021/jp2042526

Hu, Y., Jensen, J. O., Zhang, W., Cleemann, L. N., Xing, W., Bjerrum, N. J., & Li, Q. (2014). Hollow Spheres of Iron Carbide Nanoparticles Encased in Graphitic Layers as Oxygen Reduction Catalysts. *Angewandte Chemie International Edition*, *53*(14), 3675–3679. https://doi.org/10.1002/anie.201400358

Hyun, J., & Kim, H.-T. (2023). Powering the hydrogen future: Current status and challenges of anion exchange membrane fuel cells. *Energy & Environmental Science*, *16*(12), 5633–5662. https://doi.org/10.1039/D3EE01768K

Iijima1991.pdf. (n.d.).

Inagaki, M., Kobayashi, S., Kojin, F., Tanaka, N., Morishita, T., & Tryba, B. (2004). Pore structure of carbons coated on ceramic particles. *Carbon*, *42*(15), 3153–3158. https://doi.org/10.1016/j.carbon.2004.07.029

Jaggers, R. W., Chen, R., & Bon, S. A. F. (2016). Control of vesicle membrane permeability with catalytic particles. *Materials Horizons*, *3*(1), 41–46. https://doi.org/10.1039/C5MH00093A

Jahnke, H., Schönborn, M., & Zimmermann, G. (1976). Organic dyestuffs as catalysts for fuel cells. In F. P. Schäfer, H. Gerischer, F. Willig, H. Meier, H. Jahnke, M. Schönborn, & G. Zimmermann (Eds.), *Physical and Chemical Applications of Dyestuffs* (Vol. 61, pp. 133–181). Springer-Verlag. https://doi.org/10.1007/BFb0046059

Jänes, A., Thomberg, T., Kurig, H., & Lust, E. (2009). Nanoscale fine-tuning of porosity of carbide-derived carbon prepared from molybdenum carbide. *Carbon*, *47*(1), 23–29. https://doi.org/10.1016/j.carbon.2008.07.010

Jasinski, R. (1965). Cobalt Phthalocyanine as a Fuel Cell Cathode. *Journal of The Electrochemical Society*, *112*(5), 526. https://doi.org/10.1149/1.2423590

Jia, Q., Ramaswamy, N., Hafiz, H., Tylus, U., Strickland, K., Wu, G., Barbiellini, B., Bansil, A., Holby, E. F., Zelenay, P., & Mukerjee, S. (2015). Experimental Observation of Redox-Induced Fe–N Switching Behavior as a Determinant Role for Oxygen Reduction Activity. *ACS Nano*, *9*(12), 12496–12505. https://doi.org/10.1021/acsnano.5b05984

Jia, Q., Ramaswamy, N., Tylus, U., Strickland, K., Li, J., Serov, A., Artyushkova, K., Atanassov, P., Anibal, J., Gumeci, C., Barton, S. C., Sougrati, M.-T., Jaouen, F., Halevi, B., & Mukerjee, S. (2016). Spectroscopic insights into the nature of active sites in iron–nitrogen–carbon electrocatalysts for oxygen reduction in acid. *Nano Energy*, *29*, 65–82. https://doi.org/10.1016/j.nanoen.2016.03.025

Jiang, Z., Yu, J., Huang, T., & Sun, M. (2018). Recent Advance on Polyaniline or Polypyrrole-Derived Electrocatalysts for Oxygen Reduction Reaction. *Polymers*, *10*(12), Article 12. https://doi.org/10.3390/polym10121397

Kabir, S., Artyushkova, K., Serov, A., & Atanassov, P. (2018). Role of Nitrogen Moieties in N-Doped 3D-Graphene Nanosheets for Oxygen Electroreduction in Acidic and Alkaline Media. *ACS Applied Materials & Interfaces*, *10*(14), 11623–11632. https://doi.org/10.1021/acsami.7b18651

Kisand, K., Sarapuu, A., Douglin, J. C., Kikas, A., Treshchalov, A., Käärik, M., Piirsoo, H.-M., Paiste, P., Aruväli, J., Leis, J., Kisand, V., Tamm, A., Dekel, D. R., & Tammeveski, K. (2022). Templated Nitrogen-, Iron-, and Cobalt-Doped Mesoporous Nanocarbon Derived from an Alkylresorcinol Mixture for Anion-Exchange Membrane Fuel Cell Application. *ACS Catalysis*, *12*(22), 14050–14061. https://doi.org/10.1021/acscatal.2c03683

Koyuturk, B., Farber, E. M., Wagner, F. E., Fellinger, T.-P., & Eisenberg, D. (2022). A simple decagram-scale synthesis of an atomically dispersed, hierarchically porous Fe–N–C catalyst for acidic ORR. *Journal of Materials Chemistry A*, *10*(37), 19859–19867. https://doi.org/10.1039/D2TA00925K

Kruusenberg, I., Alexeyeva, N., Tammeveski, K., Kozlova, J., Matisen, L., Sammelselg, V., Solla-Gullón, J., & Feliu, J. M. (2011). Effect of purification of carbon nanotubes on their electrocatalytic properties for oxygen reduction in acid solution. *Carbon*, *49*(12), 4031–4039. https://doi.org/10.1016/j.carbon.2011.05.048

Kruusenberg, I., Ramani, D., Ratso, S., Joost, U., Saar, R., Rauwel, P., Kannan, A. M., & Tammeveski, K. (2016). Cobalt–Nitrogen Co-doped Carbon Nanotube Cathode Catalyst

for Alkaline Membrane Fuel Cells. *ChemElectroChem*, *3*(9), 1455–1465. https://doi.org/10.1002/celc.201600241

Kumar, K., Gairola, P., Lions, M., Ranjbar-Sahraie, N., Mermoux, M., Dubau, L., Zitolo, A., Jaouen, F., & Maillard, F. (2018). Physical and Chemical Considerations for Improving Catalytic Activity and Stability of Non-Precious-Metal Oxygen Reduction Reaction Catalysts. *ACS Catalysis*, *8*(12), 11264–11276. https://doi.org/10.1021/acscatal.8b02934

Lefèvre, M., Proietti, E., Jaouen, F., & Dodelet, J.-P. (2009). Iron-Based Catalysts with Improved Oxygen Reduction Activity in Polymer Electrolyte Fuel Cells. *Science*, *324*(5923), 71–74. https://doi.org/10.1126/science.1170051

Leis, J., Arulepp, M., Käärik, M., & Perkson, A. (2010). The effect of Mo2C derived carbon pore size on the electrical double-layer characteristics in propylene carbonate-based electrolyte. *Carbon*, *48*(14), 4001–4008. https://doi.org/10.1016/j.carbon.2010.07.003

Leis, J., Perkson, A., Arulepp, M., Käärik, M., & Svensson, G. (2001). Carbon nanostructures produced by chlorinating aluminium carbide. *Carbon*, *39*(13), 2043–2048. https://doi.org/10.1016/S0008-6223(01)00020-3

Li, J., Chen, M., Cullen, D. A., Hwang, S., Wang, M., Li, B., Liu, K., Karakalos, S., Lucero, M., Zhang, H., Lei, C., Xu, H., Sterbinsky, G. E., Feng, Z., Su, D., More, K. L., Wang, G., Wang, Z., & Wu, G. (2018a). Atomically dispersed manganese catalysts for oxygen reduction in proton-exchange membrane fuel cells. *Nature Catalysis*, *1*(12), 935–945. https://doi.org/10.1038/s41929-018-0164-8

Li, J., Chen, M., Cullen, D. A., Hwang, S., Wang, M., Li, B., Liu, K., Karakalos, S., Lucero, M., Zhang, H., Lei, C., Xu, H., Sterbinsky, G. E., Feng, Z., Su, D., More, K. L., Wang, G., Wang, Z., & Wu, G. (2018b). Atomically dispersed manganese catalysts for oxygen reduction in proton-exchange membrane fuel cells. *Nature Catalysis*, *1*(12), 935–945. https://doi.org/10.1038/s41929-018-0164-8

Li, Q., Xu, D., Ou, X., & Yan, F. (2017). Nitrogen-Doped Graphitic Porous Carbon Nanosheets Derived from In Situ Formed g-C_3N_4 Templates for the Oxygen Reduction Reaction. *Chemistry – An Asian Journal*, *12*(14), 1816–1823. https://doi.org/10.1002/asia.201700586

Lin, Z., Song, M., Ding, Y., Liu, Y., Liu, M., & Wong, C. (2012). Facile preparation of nitrogen-doped graphene as a metal-free catalyst for oxygen reduction reaction. *Physical Chemistry Chemical Physics*, *14*(10), 3381. https://doi.org/10.1039/c2cp00032f

Liu, R., Wu, D., Feng, X., & Müllen, K. (2010). Nitrogen-Doped Ordered Mesoporous Graphitic Arrays with High Electrocatalytic Activity for Oxygen Reduction. *Angewandte Chemie International Edition*, *49*(14), 2565–2569. https://doi.org/10.1002/anie.200907289

Liu, X., Wang, X., Licht, G., & Licht, S. (2020). Transformation of the greenhouse gas carbon dioxide to graphene. *Journal of CO2 Utilization*, *36*, 288–294. https://doi.org/10.1016/j.jcou.2019.11.019

Ma, Y., Sun, L., Huang, W., Zhang, L., Zhao, J., Fan, Q., & Huang, W. (2011). Three-Dimensional Nitrogen-Doped Carbon Nanotubes/Graphene Structure Used as a Metal-Free Electrocatalyst for the Oxygen Reduction Reaction. *The Journal of Physical Chemistry C*, *115*(50), 24592–24597. https://doi.org/10.1021/jp207736h

Mamtani, K., Jain, D., Zemlyanov, D., Celik, G., Luthman, J., Renkes, G., Co, A. C., & Ozkan, U. S. (2016). Probing the Oxygen Reduction Reaction Active Sites over Nitrogen-Doped Carbon Nanostructures (CN_x) in Acidic Media Using Phosphate Anion. *ACS Catalysis*, *6*(10), 7249–7259. https://doi.org/10.1021/acscatal.6b01786

Matanovic, I., Artyushkova, K., & Atanassov, P. (2018). Understanding PGM-free catalysts by linking density functional theory calculations and structural analysis: Perspectives and challenges. *Current Opinion in Electrochemistry*, *9*, 137–144. https://doi.org/10.1016/j.coelec.2018.03.009

Matthey, J. (2019). *Pgm Market Report May 2019*.

Meng, H., Larouche, N., Lefèvre, M., Jaouen, F., Stansfield, B., & Dodelet, J.-P. (2010). Iron porphyrin-based cathode catalysts for polymer electrolyte membrane fuel cells: Effect of NH3 and Ar mixtures as pyrolysis gases on catalytic activity and stability. *Electrochimica Acta*, *55*(22), 6450–6461. https://doi.org/10.1016/j.electacta.2010.06.039

Menga, D., Low, J. L., Li, Y.-S., Arčon, I., Koyutürk, B., Wagner, F., Ruiz-Zepeda, F., Gaberšček, M., Paulus, B., & Fellinger, T.-P. (2021). Resolving the Dilemma of Fe–N–C Catalysts by the Selective Synthesis of Tetrapyrrolic Active Sites via an Imprinting Strategy. *Journal of the American Chemical Society*, *143*(43), 18010–18019. https://doi.org/10.1021/jacs.1c04884

Menga, D., Ruiz-Zepeda, F., Moriau, L., Šala, M., Wagner, F., Koyutürk, B., Bele, M., Petek, U., Hodnik, N., Gaberšček, M., & Fellinger, T. (2019). Active-Site Imprinting: Preparation of Fe–N–C Catalysts from Zinc Ion–Templated Ionothermal Nitrogen-Doped Carbons. *Advanced Energy Materials*, *9*(43), 1902412. https://doi.org/10.1002/aenm.201902412

Mineva, T., Matanovic, I., Atanassov, P., Sougrati, M.-T., Stievano, L., Clémancey, M., Kochem, A., Latour, J.-M., & Jaouen, F. (2019). Understanding Active Sites in Pyrolyzed Fe–N–C Catalysts for Fuel Cell Cathodes by Bridging Density Functional Theory Calculations and ^{57} Fe Mössbauer Spectroscopy. *ACS Catalysis*, *9*(10), 9359–9371. https://doi.org/10.1021/acscatal.9b02586

Monteverde Videla, A. H. A., Sebastián, D., Vasile, N. S., Osmieri, L., Aricò, A. S., Baglio, V., & Specchia, S. (2016). Performance analysis of Fe–N–C catalyst for DMFC cathodes: Effect of water saturation in the cathodic catalyst layer. *International Journal of Hydrogen Energy*, *41*(47), 22605–22618. https://doi.org/10.1016/j.ijhydene.2016.06.060

Mufundirwa, A., Harrington, G. F., Smid, B., Cunning, B. V., Sasaki, K., & Lyth, S. M. (2018). Durability of template-free Fe-N-C foams for electrochemical oxygen reduction in alkaline solution. *Journal of Power Sources*, *375*, 244–254. https://doi.org/10.1016/j.jpowsour.2017.07.025

Mustain, W. E. (2018). Understanding how high-performance anion exchange membrane fuel cells were achieved: Component, interfacial, and cell-level factors. *Current Opinion in Electrochemistry*, *12*, 233–239. https://doi.org/10.1016/j.coelec.2018.11.010

Nazir, H., Louis, C., Jose, S., Prakash, J., Muthuswamy, N., Buan, M. E. M., Flox, C., Chavan, S., Shi, X., Kauranen, P., Kallio, T., Maia, G., Tammeveski, K., Lymperopoulos, N., Carcadea, E., Veziroglu, E., Iranzo, A., & Kannan, A. M. (2020). Is the H2 economy realizable in the foreseeable future? Part I: H2 production methods. *International Journal*

of Hydrogen Energy, *45*(27), 13777–13788. https://doi.org/10.1016/j.ijhydene.2020.03.092

Niwa, H., Horiba, K., Harada, Y., Oshima, M., Ikeda, T., Terakura, K., Ozaki, J., & Miyata, S. (2009). X-ray absorption analysis of nitrogen contribution to oxygen reduction reaction in carbon alloy cathode catalysts for polymer electrolyte fuel cells. *Journal of Power Sources*, *187*(1), 93–97. https://doi.org/10.1016/j.jpowsour.2008.10.064

Niyogi, S., Hamon, M. A., Hu, H., Zhao, B., Bhowmik, P., Sen, R., Itkis, M. E., & Haddon, R. C. (2002). Chemistry of Single-Walled Carbon Nanotubes. *Accounts of Chemical Research*, *35*(12), 1105–1113. https://doi.org/10.1021/ar010155r

Novoselov, K. S., Geim, A. K., Morozov, S. V., Jiang, D., Zhang, Y., Dubonos, S. V., Grigorieva, I. V., & Firsov, A. A. (2004). Electric Field Effect in Atomically Thin Carbon Films. *Science*, *306*(5696), 666–669. https://doi.org/10.1126/science.1102896

Ong, A. L., Inglis, K. K., Whelligan, D. K., Murphy, S., & Varcoe, J. R. (2015). Effect of cationic molecules on the oxygen reduction reaction on fuel cell grade Pt/C (20 wt%) catalyst in potassium hydroxide (aq, 1 mol dm $^{-3}$). *Physical Chemistry Chemical Physics*, *17*(18), 12135–12145. https://doi.org/10.1039/C4CP04973J

Osmieri, L., Park, J., Cullen, D. A., Zelenay, P., Myers, D. J., & Neyerlin, K. C. (2021). Status and challenges for the application of platinum group metal-free catalysts in proton-exchange membrane fuel cells. *Current Opinion in Electrochemistry*, *25*, 100627. https://doi.org/10.1016/j.coelec.2020.08.009

Osmieri, L., Pezzolato, L., & Specchia, S. (2018). Recent trends on the application of PGM-free catalysts at the cathode of anion exchange membrane fuel cells. *Current Opinion in Electrochemistry*, *9*, 240–256. https://doi.org/10.1016/j.coelec.2018.05.011

Pampel, J., Denton, C., & Fellinger, T.-P. (2016). Glucose derived ionothermal carbons with tailor-made porosity. *Carbon*, *107*, 288–296. https://doi.org/10.1016/j.carbon.2016.06.009

Parvez, K., Yang, S., Hernandez, Y., Winter, A., Turchanin, A., Feng, X., & Müllen, K. (2012). Nitrogen-Doped Graphene and Its Iron-Based Composite As Efficient Electrocatalysts for Oxygen Reduction Reaction. *ACS Nano*, *6*(11), 9541–9550. https://doi.org/10.1021/nn302674k

Pavlenko, V., Khosravi H, S., Żółtowska, S., Haruna, A. B., Zahid, M., Mansurov, Z., Supiyeva, Z., Galal, A., Ozoemena, K. I., Abbas, Q., & Jesionowski, T. (2022). A comprehensive review of template-assisted porous carbons: Modern preparation methods and advanced applications. *Materials Science and Engineering: R: Reports*, *149*, 100682. https://doi.org/10.1016/j.mser.2022.100682

Peng, L., Xu, Z., Liu, Z., Wei, Y., Sun, H., Li, Z., Zhao, X., & Gao, C. (2015). An iron-based green approach to 1-h production of single-layer graphene oxide. *Nature Communications*, *6*(1), 5716. https://doi.org/10.1038/ncomms6716

Ping, K., Braschinsky, A., Alam, M., Bhadoria, R., Mikli, V., Mere, A., Aruväli, J., Paiste, P., Vlassov, S., Kook, M., Rähn, M., Sammelselg, V., Tammeveski, K., Kongi, N., & Starkov, P. (2020). Fused Hybrid Linkers for Metal–Organic Framework-Derived Bifunctional Oxygen Electrocatalysts. *ACS Applied Energy Materials*, *3*(1), 152–157. https://doi.org/10.1021/acsaem.9b02039

Pollet, B. G., Kocha, S. S., & Staffell, I. (2019). Current status of automotive fuel cells for sustainable transport. *Current Opinion in Electrochemistry*, *16*, 90–95. https://doi.org/10.1016/j.coelec.2019.04.021

Primbs, M., Sun, Y., Roy, A., Malko, D., Mehmood, A., Sougrati, M.-T., Blanchard, P.-Y., Granozzi, G., Kosmala, T., Daniel, G., Atanassov, P., Sharman, J., Durante, C., Kucernak, A., Jones, D., Jaouen, F., & Strasser, P. (2020). Establishing reactivity descriptors for platinum group metal (PGM)-free Fe–N–C catalysts for PEM fuel cells. *Energy & Environmental Science*, *13*(8), 2480–2500. https://doi.org/10.1039/D0EE01013H

Proietti, E., Jaouen, F., Lefèvre, M., Larouche, N., Tian, J., Herranz, J., & Dodelet, J.-P. (2011). Iron-based cathode catalyst with enhanced power density in polymer electrolyte membrane fuel cells. *Nature Communications*, *2*(1), 416. https://doi.org/10.1038/ncomms1427

Ramaswamy, N., & Mukerjee, S. (2012). Fundamental Mechanistic Understanding of Electrocatalysis of Oxygen Reduction on Pt and Non-Pt Surfaces: Acid versus Alkaline Media. *Advances in Physical Chemistry*, *2012*, 1–17. https://doi.org/10.1155/2012/491604

Rao, C. V., Cabrera, C. R., & Ishikawa, Y. (2010). In Search of the Active Site in Nitrogen-Doped Carbon Nanotube Electrodes for the Oxygen Reduction Reaction. *The Journal of Physical Chemistry Letters*, *1*(18), 2622–2627. https://doi.org/10.1021/jz100971v

Ratso, S. (2020). *Electrocatalysis of oxygen reduction on non-precious metal catalysts*. http://hdl.handle.net/10062/70698

Ratso, S. (2020). *Electrocatalysis of oxygen reduction on non-precious metal catalysts*. http://hdl.handle.net/10062/70698

Ratso, S., Kruusenberg, I., Joost, U., Saar, R., & Tammeveski, K. (2016). Enhanced oxygen reduction reaction activity of nitrogen-doped graphene/multi-walled carbon nanotube catalysts in alkaline media. *International Journal of Hydrogen Energy*, *41*(47), 22510–22519. https://doi.org/10.1016/j.ijhydene.2016.02.021

Sahraie, N. R., Kramm, U. I., Steinberg, J., Zhang, Y., Thomas, A., Reier, T., Paraknowitsch, J.-P., & Strasser, P. (2015). Quantifying the density and utilization of active sites in non-precious metal oxygen electroreduction catalysts. *Nature Communications*, *6*(1), 8618. https://doi.org/10.1038/ncomms9618

Santori, P. G., Speck, F. D., Cherevko, S., Firouzjaie, H. A., Peng, X., Mustain, W. E., & Jaouen, F. (2020). High Performance FeNC and Mn-oxide/FeNC Layers for AEMFC Cathodes. *Journal of The Electrochemical Society*, *167*(13), 134505. https://doi.org/10.1149/1945-7111/abb7e0

Sarapuu, A., Kibena-Põldsepp, E., Borghei, M., & Tammeveski, K. (2018). Electrocatalysis of oxygen reduction on heteroatom-doped nanocarbons and transition metal-nitrogen-carbon catalysts for alkaline membrane fuel cells. *Journal of Materials Chemistry A*, *6*(3), 776–804. https://doi.org/10.1039/c7ta08690c

Sarapuu, A., Samolberg, L., Kreek, K., Koel, M., Matisen, L., & Tammeveski, K. (2015). Cobalt- and iron-containing nitrogen-doped carbon aerogels as non-precious metal catalysts for electrochemical reduction of oxygen. *Journal of Electroanalytical Chemistry*, *746*, 9–17. https://doi.org/10.1016/j.jelechem.2015.03.021

Schmirler, M., Knorr, T., Fey, T., Lynen, A., Greil, P., & Etzold, B. J. M. (2011). Fast production of monolithic carbide-derived carbons with secondary porosity produced by chlorination

of carbides containing a free metal phase. *Carbon*, *49*(13), 4359–4367. https://doi.org/10.1016/j.carbon.2011.06.013

Serov, A., Artyushkova, K., Niangar, E., Wang, C., Dale, N., Jaouen, F., Sougrati, M.-T., Jia, Q., Mukerjee, S., & Atanassov, P. (2015). Nano-structured non-platinum catalysts for automotive fuel cell application. *Nano Energy*, *16*, 293–300. https://doi.org/10.1016/j.nanoen.2015.07.002

Shao, M., Chang, Q., Dodelet, J.-P., & Chenitz, R. (2016). Recent Advances in Electrocatalysts for Oxygen Reduction Reaction. *Chemical Reviews*, *116*(6), 3594–3657. https://doi.org/10.1021/acs.chemrev.5b00462

Shen, Q., Liu, X., & Jin, W. (2013). Solubility increase of multi-walled carbon nanotubes in water. *Carbon*, *60*, 562–563. https://doi.org/10.1016/j.carbon.2013.04.022

Strickland, K., Miner, E., Jia, Q., Tylus, U., Ramaswamy, N., Liang, W., Sougrati, M.-T., Jaouen, F., & Mukerjee, S. (2015). Highly active oxygen reduction non-platinum group metal electrocatalyst without direct metal–nitrogen coordination. *Nature Communications*, *6*(1), 7343. https://doi.org/10.1038/ncomms8343

Tammeveski, K., & Zagal, J. H. (2018). Electrocatalytic oxygen reduction on transition metal macrocyclic complexes for anion exchange membrane fuel cell application. *Current Opinion in Electrochemistry*, *9*, 207–213. https://doi.org/10.1016/j.coelec.2018.04.001

Tang, C., & Zhang, Q. (2017). Nanocarbon for Oxygen Reduction Electrocatalysis: Dopants, Edges, and Defects. *Advanced Materials*, *29*(13), 1604103. https://doi.org/10.1002/adma.201604103

Tao, H., Fan, Q., Ma, T., Liu, S., Gysling, H., Texter, J., Guo, F., & Sun, Z. (2020). Two-dimensional materials for energy conversion and storage. *Progress in Materials Science*, *111*, 100637. https://doi.org/10.1016/j.pmatsci.2020.100637

Thompson, S. T., & Papageorgopoulos, D. (2019). Platinum group metal-free catalysts boost cost competitiveness of fuel cell vehicles. *Nature Catalysis*, *2*(7), Article 7. https://doi.org/10.1038/s41929-019-0291-x

Tian, J., Morozan, A., Sougrati, M. T., Lefèvre, M., Chenitz, R., Dodelet, J.-P., Jones, D., & Jaouen, F. (2013). Optimized synthesis of Fe/N/C cathode catalysts for PEM fuel cells: A matter of iron-ligand coordination strength. *Angewandte Chemie (International Ed. in English)*, *52*(27), 6867–6870. https://doi.org/10.1002/anie.201303025

Trogadas, P., Fuller, T. F., & Strasser, P. (2014). Carbon as catalyst and support for electrochemical energy conversion. *Carbon*, *75*, 5–42. https://doi.org/10.1016/j.carbon.2014.04.005

Uddin, A., Dunsmore, L., Zhang, H., Hu, L., Wu, G., & Litster, S. (2020). High Power Density Platinum Group Metal-free Cathodes for Polymer Electrolyte Fuel Cells. *ACS Applied Materials & Interfaces*, *12*(2), 2216–2224. https://doi.org/10.1021/acsami.9b13945

Ul Hassan, N., Mandal, M., Huang, G., Firouzjaie, H. A., Kohl, P. A., & Mustain, W. E. (2020). Achieving High-Performance and 2000 h Stability in Anion Exchange Membrane Fuel Cells by Manipulating Ionomer Properties and Electrode Optimization. *Advanced Energy Materials*, *10*(40), 2001986. https://doi.org/10.1002/aenm.202001986

Vikkisk, M., Kruusenberg, I., Joost, U., Shulga, E., Kink, I., & Tammeveski, K. (2014). Electrocatalytic oxygen reduction on nitrogen-doped graphene in alkaline media. *Applied Catalysis B: Environmental*, *147*, 369–376. https://doi.org/10.1016/j.apcatb.2013.09.011

Vikkisk, M., Kruusenberg, I., Ratso, S., Joost, U., Shulga, E., Kink, I., Rauwel, P., & Tammeveski, K. (2015). Enhanced electrocatalytic activity of nitrogen-doped multi-walled carbon nanotubes towards the oxygen reduction reaction in alkaline media. *RSC Advances*, *5*(73), 59495–59505. https://doi.org/10.1039/C5RA08818F

Wagner, F. T., Lakshmanan, B., & Mathias, M. F. (2010). Electrochemistry and the Future of the Automobile. *The Journal of Physical Chemistry Letters*, *1*(14), 2204–2219. https://doi.org/10.1021/jz100553m

Wang, H., Maiyalagan, T., & Wang, X. (2012). Review on Recent Progress in Nitrogen-Doped Graphene: Synthesis, Characterization, and Its Potential Applications. *ACS Catalysis*, *2*(5), 781–794. https://doi.org/10.1021/cs200652y

Wang, X. X., Cullen, D. A., Pan, Y., Hwang, S., Wang, M., Feng, Z., Wang, J., Engelhard, M. H., Zhang, H., He, Y., Shao, Y., Su, D., More, K. L., Spendelow, J. S., & Wu, G. (2018). Nitrogen-Coordinated Single Cobalt Atom Catalysts for Oxygen Reduction in Proton Exchange Membrane Fuel Cells. *Advanced Materials*, *30*(11), 1706758. https://doi.org/10.1002/adma.201706758

Wang, X., Zhu, H., Yang, C., Lu, J., Zheng, L., & Liang, H.-P. (2022). Mesoporous carbon promoting the efficiency and stability of single atomic electrocatalysts for oxygen reduction reaction. *Carbon*, *191*, 393–402. https://doi.org/10.1016/j.carbon.2022.01.057

Wang, X., Zou, L., Fu, H., Xiong, Y., Tao, Z., Zheng, J., & Li, X. (2016). Noble Metal-Free Oxygen Reduction Reaction Catalysts Derived from Prussian Blue Nanocrystals Dispersed in Polyaniline. *ACS Applied Materials & Interfaces*, *8*(13), 8436–8444. https://doi.org/10.1021/acsami.5b12102

Wei, W., Liang, H., Parvez, K., Zhuang, X., Feng, X., & Müllen, K. (2014). Nitrogen-Doped Carbon Nanosheets with Size-Defined Mesopores as Highly Efficient Metal-Free Catalyst for the Oxygen Reduction Reaction. *Angewandte Chemie International Edition*, *53*(6), 1570–1574. https://doi.org/10.1002/anie.201307319

Wiggins-Camacho, J. D., & Stevenson, K. J. (2011). Mechanistic Discussion of the Oxygen Reduction Reaction at Nitrogen-Doped Carbon Nanotubes. *The Journal of Physical Chemistry C*, *115*(40), 20002–20010. https://doi.org/10.1021/jp205336w

Wohlgemuth, S.-A., White, R. J., Willinger, M.-G., Titirici, M.-M., & Antonietti, M. (2012). A one-pot hydrothermal synthesis of sulfur and nitrogen doped carbon aerogels with enhanced electrocatalytic activity in the oxygen reduction reaction. *Green Chemistry*, *14*(5), 1515. https://doi.org/10.1039/c2gc35309a

Wu, G., More, K. L., Johnston, C. M., & Zelenay, P. (2011). High-Performance Electrocatalysts for Oxygen Reduction Derived from Polyaniline, Iron, and Cobalt. *Science*, *332*(6028), 443–447. https://doi.org/10.1126/science.1200832

Wu, G., & Zelenay, P. (2013). Nanostructured Nonprecious Metal Catalysts for Oxygen Reduction Reaction. *Accounts of Chemical Research*, *46*(8), 1878–1889. https://doi.org/10.1021/ar400011z

Yadav, R. M., Wu, J., Kochandra, R., Ma, L., Tiwary, C. S., Ge, L., Ye, G., Vajtai, R., Lou, J., & Ajayan, P. M. (2015). Carbon Nitrogen Nanotubes as Efficient Bifunctional Electrocatalysts for Oxygen Reduction and Evolution Reactions. *ACS Applied Materials & Interfaces*, *7*(22), 11991–12000. https://doi.org/10.1021/acsami.5b02032

Yang, L., Shui, J., Du, L., Shao, Y., Liu, J., Dai, L., & Hu, Z. (2019). Carbon-Based Metal-Free ORR Electrocatalysts for Fuel Cells: Past, Present, and Future. *Advanced Materials*, *31*(13), 1804799. https://doi.org/10.1002/adma.201804799

Yang, Z., Nie, H., Chen, X., Chen, X., & Huang, S. (2013). Recent progress in doped carbon nanomaterials as effective cathode catalysts for fuel cell oxygen reduction reaction. *Journal of Power Sources*, *236*, 238–249. https://doi.org/10.1016/j.jpowsour.2013.02.057

Yeager, E. (1984). Electrocatalysts for O2 reduction. *Electrochimica Acta*, *29*(11), 1527–1537. https://doi.org/10.1016/0013-4686(84)85006-9

Zagal, J. H., & Bedioui, F. (Eds.). (2006). *N4-macrocyclic metal complexes*. Springer.

Zagal, J. H., & Bedioui, F. (Eds.). (2016). *Electrochemistry of N4 Macrocyclic Metal Complexes*. Springer International Publishing. https://doi.org/10.1007/978-3-319-31172-2

Zagal, J. H., & Koper, M. T. M. (2016). Reactivity Descriptors for the Activity of Molecular MN4 Catalysts for the Oxygen Reduction Reaction. *Angewandte Chemie International Edition*, *55*(47), 14510–14521. https://doi.org/10.1002/anie.201604311

Zhai, Y., Dou, Y., Zhao, D., Fulvio, P. F., Mayes, R. T., & Dai, S. (2011). Carbon Materials for Chemical Capacitive Energy Storage. *Advanced Materials*, *23*(42), 4828–4850. https://doi.org/10.1002/adma.201100984

Zhang, G., Chenitz, R., Lefèvre, M., Sun, S., & Dodelet, J.-P. (2016). Is iron involved in the lack of stability of Fe/N/C electrocatalysts used to reduce oxygen at the cathode of PEM fuel cells? *Nano Energy*, *29*, 111–125. https://doi.org/10.1016/j.nanoen.2016.02.038

Zhang, H., Hwang, S., Wang, M., Feng, Z., Karakalos, S., Luo, L., Qiao, Z., Xie, X., Wang, C., Su, D., Shao, Y., & Wu, G. (2017). Single Atomic Iron Catalysts for Oxygen Reduction in Acidic Media: Particle Size Control and Thermal Activation. *Journal of the American Chemical Society*, *139*. https://doi.org/10.1021/jacs.7b06514

Zhao, Y., Yang, L., Chen, S., Wang, X., Ma, Y., Wu, Q., Jiang, Y., Qian, W., & Hu, Z. (2013). Can Boron and Nitrogen Co-doping Improve Oxygen Reduction Reaction Activity of Carbon Nanotubes? *Journal of the American Chemical Society*, *135*(4), 1201–1204. https://doi.org/10.1021/ja310566z

Zhou, Y., Tao, X., Chen, G., Lu, R., Wang, D., Chen, M.-X., Jin, E., Yang, J., Liang, H.-W., Zhao, Y., Feng, X., Narita, A., & Müllen, K. (2020). Multilayer stabilization for fabricating high-loading single-atom catalysts. *Nature Communications*, *11*(1), 5892. https://doi.org/10.1038/s41467-020-19599-8

Zion, N., Cullen, D. A., Zelenay, P., & Elbaz, L. (2020). Heat-Treated Aerogel as a Catalyst for the Oxygen Reduction Reaction. *Angewandte Chemie International Edition*, *59*(6), 2483–2489. https://doi.org/10.1002/anie.201913521

Zitolo, A., Goellner, V., Armel, V., Sougrati, M.-T., Mineva, T., Stievano, L., Fonda, E., & Jaouen, F. (2015a). Identification of catalytic sites for oxygen reduction in iron- and nitrogen-doped graphene materials. *Nature Materials*, *14*(9), 937–942. https://doi.org/10.1038/nmat4367

Zitolo, A., Goellner, V., Armel, V., Sougrati, M.-T., Mineva, T., Stievano, L., Fonda, E., & Jaouen, F. (2015b). Identification of catalytic sites for oxygen reduction in iron- and nitrogen-doped graphene materials. *Nature Materials*, *14*(9), 937–942. https://doi.org/10.1038/nmat4367

Zitolo, A., Ranjbar-Sahraie, N., Mineva, T., Li, J., Jia, Q., Stamatin, S., Harrington, G. F., Lyth, S. M., Krtil, P., Mukerjee, S., Fonda, E., & Jaouen, F. (2017). Identification of catalytic sites in cobalt-nitrogen-carbon materials for the oxygen reduction reaction. *Nature Communications*, *8*(1), 957. https://doi.org/10.1038/s41467-017-01100-7

Acknowledgments

I would like to extend my sincerest thanks to my supervisors, M.Sc. Kaarel Kisand and Professor Kaido Tammeveski, whose exceptional guidance and unwavering support have been pivotal in the successful completion of this thesis. M.Sc. Kaarel Kisand, in particular, went the extra mile for me, taking the time to explain numerous concepts and providing extraordinary support and kindness. His profound expertise and thoughtful insights provided a seamless path through the complexities of this research. I am immensely grateful for their patience, encouragement, and the wealth of knowledge they have imparted to me throughout this journey.

Additionally, I would like to extend my appreciation to all the researchers at the Institute of Physics at the University of Tartu, Institute of Chemistry, Institure of ecology and earth science and Israel Institure of Technology, who have contributed to this bachelor's thesis. Their hard work and collaboration have been greatly valued and have played a significant role in the completion of this project.

I am deeply thankful to my wife, Azizah Bello, for her unwavering support and understanding throughout this endeavor. Her encouragement and love have been a constant source of strength. I also wish to express my gratitude to my brothers, Saheed Ibrahim and Sheriff Ibrahim, and my lovely sister, Aisha Ibrahim, for their support and encouragement.

Special thanks to my nephews, Zayyad Ibrahim and Ahmad Ibrahim, and my nieces, Su'ad Ibrahim and Maryam Mustapha, whose smiles and joy have been a source of inspiration. My heartfelt appreciation goes to my parents, Mr. Rabiu Ibrahim and Mrs. Kudirat Ibrahim, for their lifelong support and guidance, which have been the foundation of all my achievements.

Finally, I would like to thank the Institute of Technology for providing the necessary resources and a conducive environment for my research.

Appendix

I. Glossary

Caret The bar (or other symbol) marking the active editing point.	Sisestusmärk Märk, mis märgib teksti sisestamise asukohta.
Template A gauge, pattern, or mold, commonly a thin plate or board, used as a guide to the form of the work to be executed.	Mall Näidik, muster või valuvorm, mis esitab täitmisele võetava töö struktuuri.

NON-EXCLUSIVE LICENCE TO REPRODUCE THESIS AND MAKE THESIS PUBLIC

I, Faruq Olamilekan Ibrahim,

1. herewith grant the University of Tartu a free permit (non-exclusive licence) to reproduce, for the purpose of preservation, including for adding to the DSpace digital archives until the expiry of the term of copyright,
Non-precious metal electrocatalysts for oxygen reduction via ionothermal synthesis, supervised by MSc Kaarel Kisand and Professor Kaido Tammeveski.

2. I grant the University of Tartu a permit to make the work specified in p. 1 available to the public via the web environment of the University of Tartu, including via the DSpace digital archives, under the Creative Commons licence CC BY NC ND 3.0, which allows, by giving appropriate credit to the author, to reproduce, distribute the work and communicate it to the public, and prohibits the creation of derivative works and any commercial use of the work until the expiry of the term of copyright.

3. I am aware of the fact that the author retains the rights specified in p. 1 and 2.

4. I certify that granting the non-exclusive license does not infringe other persons' intellectual property rights or rights arising from the personal data protection legislation.

Faruq Olamilekan Ibrahim

22/05/2024